Sources of dissolved iron to oxygen minimum zone waters on the Senegalese continental margin in the tropical North Atlantic Ocean: Insights from iron isotopes

JK Klar[1,2], C Schlosser[3], JA Milton[1], EMS Woodward[4], F Lacan[2], IJ Parkinson[5], EP Achterberg[1,3], RH James[1]

(1) Ocean and Earth Science, National Oceanography Centre, University of Southampton, European Way, Southampton SO14 3ZH, UK

(2) LEGOS, Université de Toulouse, CNES, CNRS, IRD, UPS, 14 Avenue Edouard Belin, 31400 Toulouse, France

(3) GEOMAR Helmholtz Centre for Ocean Research, Wischhofstraße 1-3, 24148 Kiel, Germany

(4) Plymouth Marine Laboratory, Prospect Place, The Hoe, Plymouth PL1 3DH, UK

(5) School of Earth Sciences, University of Bristol, Queens Road, Bristol, BS8 1RJ, UK

Keywords: tropical Atlantic Ocean; iron isotopes; oxygen minimum zone; benthic iron; remineralisation; dissolved aluminium; dust; GEOTRACES

Abstract

Oxygen minimum zones (OMZs) cover extensive areas of eastern boundary ocean regions and play an important role in the cycling of the essential micronutrient iron (Fe). The isotopic composition of dissolved Fe (dFe) in shelf and slope waters on the Senegalese margin was determined to investigate the processes leading to enhanced dFe concentrations (up to 2 nM) in this tropical North Atlantic OMZ. Our results show that benthic sources of Fe inputs, characterised by low δ^{56}Fe down to -0.33 ‰, are upwelled to surface waters and recycled in the water column by remineralisation processes. We show that regeneration of sinking organic material becomes a more important dFe source with distance from the shelf and this remineralised dFe has relatively high δ^{56}Fe values (up to +0.41 ‰). Remineralisation plays an important role in in the redistribution of dFe that is mainly supplied by benthic and atmospheric inputs, although dust loading, calculated from dissolved aluminium concentrations, was low at the time of our study (0.17 to 0.7 µmol dFe m^{-2} d^{-1}). As OMZs are expected to expand, our data provide important insights into Fe sources and Fe cycling in the tropical North Atlantic Ocean.

1. Introduction

Iron (Fe) is an essential element for marine phytoplankton (Martin, 1990; Martin and Fitzwater, 1988), including nitrogen fixing diazotrophs (e.g., Berman-Frank et al., 2001; Falkowski, 1997). Iron supply therefore influences the nitrogen cycle (Schlosser et al., 2014) and the strength of the

biological carbon pump (Coale et al., 2004). Marine photosynthesis is responsible for about half of the global atmospheric CO_2 uptake (Le Quéré et al., 2013), and phytoplankton growth is limited by Fe availability in ~ 50 % of the world's ocean (Moore et al., 2001). Proper constraints on the sources of Fe to the oceans, and the processes that regulate its distribution, are essential for global models that are used to calculate past and future climate scenarios (e.g., Boyd and Ellwood, 2010).

The supply of Fe to the oceans is temporally and spatially variable. The low solubility of Fe in oxygenated seawater (pH ~8.1) (Liu and Millero, 2002), its highly particle reactive nature (Goldberg, 1954) and its uptake by marine microorganisms (Coale et al., 2004) lead to rapid removal of Fe from the surface ocean. Therefore, Fe concentrations tend to be highest close to source regions. Iron is mainly delivered to the ocean from atmospheric dust deposition, margin sediments, rivers, groundwater discharge and hydrothermal vents (Boyd and Ellwood, 2010, and references therein).

In the open ocean dissolved Fe (dFe; i.e. filterable through 0.4 or 0.2 μm) concentrations typically range between <0.2 to ~1 nmol L^{-1} (e.g., Klunder et al., 2012; Klunder et al., 2011; Nishioka and Obata, 2017; Resing et al., 2015; Rijkenberg et al., 2014) and are generally lowest in the surface ocean. However, dFe concentrations of 1 to 1.7 nmol L^{-1} have been observed within oxygen minimum zones (OMZs) (Conway and John, 2014; Fitzsimmons et al., 2013; John et al., 2017; Milne et al., 2017; Rijkenberg et al., 2012; Ussher et al., 2013; Ussher et al., 2010). Elevated biological production in surface waters caused by upwelling of nutrient rich waters in eastern boundary ocean regions results in the development of OMZs through enhanced oxygen consumption associated with sinking organic matter degradation (Karstensen et al., 2008). OMZs usually extend between ~100 and ~700 m water depth in regions with sluggish circulation and reduced ventilation, such as the eastern tropical Atlantic and eastern tropical Pacific (Stramma et al., 2005). Elevated dFe concentrations encountered in OMZs are attributed to remineralisation of biogenic Fe that sinks from the surface (Fitzsimmons et al., 2013; Rijkenberg et al., 2012), and transport of high dFe – low oxygen waters from the adjacent continental shelf forms another source (Conway and John, 2014; Ussher et al., 2010). In addition, elevated dFe concentrations off the Peru margin of the eastern tropical South Pacific have been attributed to reversible scavenging of dFe from sinking particles (John et al., 2017). The relative importance of each of these processes for Fe supply to oxygen deficient waters is, however, poorly constrained. As anthropogenic climate change results in the expansion and intensification of OMZs in the worlds' oceans (Brandt et al., 2010; Schmidtko et al., 2017; Stramma et al., 2008b) and is postulated to have important effects on the biogeochemical cycling of many redox-sensitive elements, including Fe, as well as ecosystem functioning (Chan et al., 2008; Keeling et al., 2010), the Fe sources to OMZs need to be constrained.

Iron isotopes (expressed in delta notation of the $^{56}Fe/^{54}Fe$ ratio of the sample relative to that of the reference material IRMM-014) are a relatively new tool that can help to identify Fe supply and removal mechanisms in the ocean as well as biogeochemical processing of Fe within the ocean (e.g. (Lacan et al., 2008), that cannot be provided by concentration data only. The isotopic signatures of dFe for different sources are distinct. The continental crust has an average $\delta^{56}Fe$ value of +0.09 ± 0.10 ‰ (2 SD, *n = 46*; Beard et al. (2003)). The $\delta^{56}Fe$ value of atmospheric dust in the North Atlantic (~+0.07 ± 0.11 ‰; Mead et al., 2013; Waeles et al., 2007) is similar to the crustal value, but is modified during delivery and dissolution in surface seawater, leading to a $\delta^{56}Fe$ signature of between +0.3 and +0.7 ‰ (Conway and John, 2014), although this value may be the result of other processes, such as biological uptake. Fe reduction in anoxic sediments and the efflux of pore waters supply isotopically light Fe to the overlying water column, leading to typical $\delta^{56}Fe$ values in oxygenated bottom waters of between -1.25 and -0.1 ‰ (Chever et al., 2015; Conway and John, 2014; Klar et al., 2017a), and as low as -3.5 ‰ in anoxic bottom waters (John et al., 2012). In contrast, non-reductive dissolution of lithogenic material on continental margins and in the water column is thought to lead to a $\delta^{56}Fe$ of dFe between -0.3 and +0.5 ‰ (Abadie et al., 2017; Homoky et al., 2013; Radic et al., 2011), and an isotopic difference between dissolved and particulate Fe ($\Delta^{56}Fe_{dFe\text{-}pFe}$) of +0.27 ± 0.25 ‰ (Labatut et al., 2014). The isotopic signal of river-derived dFe is +0.3 to +0.4 ‰, and is not altered during estuarine mixing with adjacent coastal waters (Bergquist and Boyle, 2006; Escoube et al., 2009; Poitrasson et al., 2014). The $\delta^{56}Fe$ values of all of these sources can nevertheless be modified by chemical and physical transformations within the ocean.

Upon delivery of Fe to the ocean from reducing sediments, rivers or hydrothermal vents, the change in ambient temperature, salinity, oxygen concentrations, pH and redox potential leads to Fe precipitation into mineral phases, such as Fe-(oxy)hydroxides and Fe-sulphides. The remaining reduced Fe (Fe(II)) after partial oxidation to Fe(III) followed by Fe(III)-(oxy)hydroxide precipitation could theoretically be up to 3.9 ‰ lighter than the initial Fe(II) pool (Klar et al., 2017b). The formation of iron sulphide (FeS) minerals leads to an isotopic fractionation of $\Delta^{56}Fe_{Fe(II)\text{-}FeS} < +0.77$ ‰ (Rouxel et al., 2008). It is now clear that dFe is rapidly complexed to organic ligands upon delivery to the ocean, with >99 % of dFe bound to organic ligands (Gledhill and Buck, 2012) and references therein). Ligand complexed Fe has $\delta^{56}Fe$ values up to 0.6 ‰ higher than inorganic dFe (Dideriksen et al., 2008; Morgan et al., 2010). In the presence of sufficient light and macronutrients, Fe is rapidly taken up by primary production in the surface ocean. Opposing directions of Fe isotopic fractionation associated with biological uptake have been reported. The uptake of isotopically light Fe with an isotopic difference between the particulate and dissolved $\delta^{56}Fe$ values, $\Delta^{56}Fe_{pFe\text{-}dFe} < -0.54$ ‰ has been observed in the waters east of New Zealand and in the equatorial Pacific Ocean (Ellwood et al.,

2015; Radic et al., 2011). In contrast, relatively low δ^{56}Fe values of dFe (-0.01 ‰) were observed in the deep fluorescence maximum and dFe minimum in the North Atlantic Ocean (Conway and John, 2014). Thus, it appears that the sinking of dead phytoplankton cells and its remineralisation at depth can lead to the release of both isotopically light (Ellwood et al., 2015; Radic et al., 2011) or heavy (Conway and John, 2014) Fe to the dissolved pool. Iron is highly particle reactive (Goldberg, 1954), and it is thought that adsorption/desorption of Fe onto/from particle surfaces is continuously occurring throughout the water column (Milne et al., 2017). The effects of scavenging/desporption on the isotopic composition of dFe are not yet clear. While one study found that scavenging resulted in the preferential uptake of heavy Fe onto particles ($\Delta^{56}Fe_{dFe\text{-}scavFe}$ = -0.67 ‰; Ellwood et al., 2015), results from another study indicated differences in δ^{56}Fe values of scavenged Fe relative to dFe were small ($\Delta^{56}Fe_{dFe\text{-}scavFe}$ = +0.3 ± 0.3 ‰; Radic et al., 2011).

To constrain the processes that regulate the behaviour of Fe within OMZs, we have determined the isotopic signature of dFe in the West African shelf and slope region of the tropical North Atlantic Ocean. We use our data to identify the sources of dFe in the OMZ and assess the effects of internal processes, such as Fe-ligand formation, biological uptake, remineralisation and scavenging, as well as water mass transport and mixing on the distribution of Fe. This work contributes to the international GEOTRACES program (www.geotraces.org).

2. Materials and methods

2.1 Cleaning procedures

Seawater samples were collected in one litre high density polyethylene (HDPE) bottles (Nalgene), which were acid cleaned following a three-step procedure. Firstly, the bottles were filled and submerged for at least 3 days in 2 % Decon. After a thorough rinse in reverse osmosis water, the bottles were filled and submerged in a 6 M hydrochloric acid (HCl, analytical grade, Fisher Scientific) bath for one week. The bottles were then rinsed with purified deionised water (Milli-Q, Merk Millipore; resistivity = 18.2 MΩ cm) and transferred into a 7 M nitric acid (HNO_3, analytical grade, Fisher Scientific) bath for another week. Finally, the bottles were thoroughly rinsed with purified deionised water, double bagged and stored in boxes until sampling on the ship.

Laboratory equipment used for sample processing was mainly polytetrafluoroethylene (PTFE) fluorinated ethylene propylene (FEP) or perfluoroalkoxy (PFA), with some low density polyethylene (LDPE) and polyethylene (PE) components, cleaned thoroughly in dilute HCl and HNO_3 before and between uses.

2.2 Sample collection

Samples were collected during RRS *Discovery* cruise D361 (GEOTRACES section GA06) between 7th February and 19th March 2011. Water was collected from four stations, ranging from 51 to 2656 m water depth (Figure 1), using a trace metal clean conductivity-temperature-pressure (CTD) rosette system. The trace metal clean CTD (TM-CTD) rosette was equipped with 24 10 L OTE (Ocean Test Equipment, Inc.) bottles (with external springs, modified for trace metal work) that were mounted onto a titanium frame. The CTD was deployed on a non-conducting Kevlar wire fitted with a Seabird auto-fire module that triggered the OTE bottles at pre-programmed depths. Sampling depths were selected according to salinity, temperature, dissolved oxygen concentration and transmission profiles, obtained immediately beforehand by a standard stainless steel CTD deployment. Immediately after recovery of the trace metal clean CTD rosette, the OTE bottles were transferred into a trace metal clean container for sub-sampling.

Water samples from the TM-CTD were filtered through 0.2 µm Acropak 500 filter capsules (Pall Corp.), that were pre-rinsed with ~5 L surface seawater from the trace metal clean 'tow-fish", or through acid cleaned 0.45 µm polyethersulfone membrane filters (Supor, Pall Gelman). The filters were rinsed with several 100 mL of sample, followed by three rinses of the HDPE sample bottle before filling up. For Fe isotopes, three 1 L bottles were filled for each sample. Filtration was carried out under oxygen-free N_2 gas with a low overpressure of 10-50 kPa.

Surface seawater samples were collected with the trace metal clean "tow-fish", deployed on the side of the ship. Seawater was pumped into the clean laboratory using a trace metal clean Teflon diaphragm pump through acid washed braided PVC tubing during the ships transit (10 knots). Samples were filtered in-line through a 0.8/0.2 µm cartridge filter (AcroPak1000) into acid-washed low-density polyethylene bottles for dFe and dAl analysis.

Samples were acidified to pH ~2 with concentrated HCl (Romil, Ultra Purity Acid, UpA). Isotope samples were double bagged and stored for shipping back to the National Oceanography Centre (NOC) in Southampton for analysis. Dissolved Al samples were allowed to equilibrate for at least 24 h prior analysis on board.

2.3 Analysis of dissolved Fe Isotopes and Fe concentrations

Iron for isotope analysis was preconcentrated using a nitriloacetic acid (NTA) Superflow resin (Qiagen) and purified by anion exchange chromatography (BioRad AG1-x8 resin). Two preconcentration protocols were used, a batch method, modified from (John and Adkins, 2010) and a column method, based on (Lacan et al., 2010). The average yield from both methods was 95 ± 8 % Fe (n = 15) and the procedure blank was 1.7 ± 0.5 ng Fe (n=11) for the batch method and 2.3 ± 0.7 ng Fe

(n=10) for the column method. Sample volumes ranged from 1 to 3 L with 100 to 350 ng Fe. When dFe concentrations were < 1.5 nmol L^{-1}, individual 1 L bottles were combined in LDPE cubitainers to increase the sample volume. Dissolved Fe concentrations were analysed on board using chemiluminescence flow-injection-analysis following a method outlined by Klunder et al. (2011) and are published in Schlosser et al. (2014) and Milne et al. (2017).

Isotopic measurements of samples were carried out in duplicate on a multi-collector inductively coupled plasma mass spectrometer (MC-ICP-MS) (Thermo Fisher Neptune) at the University of Southampton. Instrumental mass bias was corrected by addition of a double spike (45.7% ^{57}Fe, 53.1 % ^{58}Fe and 0.5 % ^{54}Fe) prior to sample processing and ^{56}Fe/^{54}Fe sample ratios are expressed as δ^{56}Fe relative to the average ^{56}Fe/^{54}Fe value for the Fe isotope reference material IRMM-014 (Institute for Reference Materials and Measurements) determined during the same analytical session. The external precision and accuracy of the isotope measurements was assessed by multiple analyses of an Fe isotope standard during each analytical session. The average value of ETH (Eidgenössische Technische Hochschule, Zürich) hematite standard for all analytical sessions was 0.52 ± 0.07 ‰ (2 SD, *n = 54*). This value compares well with previous measurements of the ETH hematite standard reported in (Lacan et al., 2010) (0.52 ± 0.08 ‰, 2 SD, *n = 81*). Analytical replicates, which consisted of splitting the sample and replicating the entire analytical procedure, yielded 2SD < 0.08 ‰ for samples 6_16 and 8_13 (Table 1).

We have further validated our Fe isotope method by blind analysis of two seawater samples that had already been analysed in F. Lacan's lab (LEGOS, Toulouse, France). The seawater samples were collected from Station 14 during Cruise R/V Kilo Moana 06252006 and Fe isotope results obtained at LEGOS are published in Radic et al. (2011). Fe concentrations were sub nano-molar, which is characteristic of open ocean seawater. We obtained δ^{56}Fe values of +0.07 ± 0.07 ‰ (*n = 2*) for sample 14-2 at 849 m depth (vs. +0.22 ± 0.05 ‰ in Radic et al., 2011) and +0.34 ± 0.06 ‰ (*n = 2*) for sample 14-6 at 198 m depth (vs +0.40 ± 0.06 ‰ in Radic et al., 2011). These replicate analyses are within the range of inter-lab reproducibility (± 0.17 ‰) at 0.4 nmol L^{-1}, reported in Boyle et al. (2012).

2.4 Analysis of dissolved aluminium concentrations

Dissolved aluminium (dAl) concentrations were determined on board by flow injection analysis using a lumogallion-Al fluorescence technique originally developed by Resing and Measures (1994) and modified according to Brown and Bruland (2008). The analytical procedure was validated by analysing North Atlantic GEOTRACES Reference Seawater. GD-23 yielded 18.2 ± 1.0 nmol kg^{-1} dAl, *n = 4* (vs a consensus value of 17.7 ± 0.2 nmol kg^{-1}) and GS-57 yielded 27.1 ± 1.1 nmol kg^{-1} dAl, *n = 5* (vs a consensus value of 27.5 ± 0.2 nmol kg^{-1}).

2.5 Auxiliary data

Salinity (conductivity), temperature, depth (pressure) and oxygen concentrations in the water column were determined using a Seabird CTD sensor mounted on the rosette frame. Sensors were cross-calibrated with discrete seawater analyses using the Winkler method for oxygen and conductivity measurements of a certified reference material for salinity. Chlorophyll-a content was monitored using a fluorometer fitted on the rosette frame and calibrated against analyses of discrete samples collected from standard CTD casts and the underway tow fish.

Concentrations of seawater nitrate, nitrite, silicate, ammonium and phosphate were determined on board the RRS *Discovery*, using a 5-channel segmented flow auto-analyser (Bran and Luebbe AAIII) (Woodward and Rees, 2001).

3. Results

3.1 Hydrography and oxygen content

Off the coast of Senegal, four main water masses were identified from potential temperature, salinity and potential density data (Figure 2). The surface 40 m consisted of Tropical Surface Water (TSW; σ_θ < 25.8 kg m^{-3}) (Stramma et al., 2008a; Stramma et al., 2005). Between the isopycnals (σ_θ) 25.8 and 27.1 kg m^{-3}, at temperatures above 8 °C, subsurface waters down to 500 m depth mainly consisted of South Atlantic Central Water (SACW) (Stramma et al., 2005). SACW is formed from Indian Ocean Central Water, which is transferred to the Atlantic Ocean by the Aghulas and Benguela currents (Stramma and England, 1999). After flowing northwards with the Benguela Current, SACW flows westward to the tropical Atlantic with the South Equatorial Current (SEC) (Stramma and Schott, 1999). Below 500 m water depth, northward flowing Antarctic Intermediate Water (AAIW) was identified by a pronounced salinity minimum at ~34.8 PSU, elevated oxygen and nutrient concentrations, and was observed at stations 2 and 3 with its core at 900 m depth (Stramma et al., 2005). Southward flowing North Atlantic Deep Water (NADW) was observed below 1200 m depth to the seafloor at Station 2 (σ_θ > 27.6 kg m^{-3}), and is characterised by its relatively high salinity (Stramma and England, 1999).

The flow field in the upper 800 m of the northeastern subtropical Atlantic is controlled by a wind driven subtropical gyre (Stramma et al., 2005) (Figure 1). Upwelling occurs near the coast of Senegal and Mauritania, as well as in the Guinea Dome (Schott et al., 2004). Coastal upwelling replaces the water moved offshore by Ekman transport, driven by equatorward winds (Stramma et al., 2005). Upwelling in the Guinea Dome is due to cyclonic circulation, associated with the North Equatorial Counter Current (NECC), the northern NECC (nNECC) and the North Equatorial Undercurrent (NEUC)

(Stramma et al., 2008a; Stramma et al., 2005) (Figure 1). The Guinea Dome and its related circulation are weakened during the winter, even though they exist throughout the year (Siedler et al., 1987).

In the upper 40 m of the water column, oxygen concentrations were > 200 µmol kg^{-1}. Oxygen concentrations were < 70 µmol kg^{-1} at depths between ~40 and ~900 m (the approximate extension of these waters at 400 m depth is shown in Figure 1). Oxygen depleted waters roughly coincided with the extension of SACW and the upper part of AAIW (Figure 2). Oxygen concentrations reached a minimum of ~ 45 µmol kg^{-1} at around 400 m depth at Stations 2 and 3. NADW was well oxygenated, and oxygen concentrations were > 200 µmol kg^{-1} near the seafloor. Our observations agree with previous reports of oxygen concentrations > 35 µmol kg^{-1} for the OMZ in the tropical North Atlantic Ocean, compared to concentrations within the OMZ of the eastern tropical Pacific Ocean being < 3 µmol kg^{-1} (Stramma et al., 2008b). The OMZ in the tropical North Atlantic Ocean consists of poorly ventilated upwelled waters, flowing westward from the African coast. The OMZ is contained by ventilation from below by AAIW; in the north and south by the eastward flowing zonal jets; and in the west by subtropical gyre waters (Stramma et al., 2005).

3.2 Distributions of dFe, δ^{56}Fe and macronutrients

Dissolved Fe concentrations in the water column ranged between 1.33 nmol L^{-1} and 6.3 nmol L^{-1} (Figure 4 and Table 1). On the shelf, the highest dFe concentrations were observed near the seafloor and lowest concentrations in the surface waters, indicating benthic supply. By contrast, the slope stations (2 and 3) showed a mid-depth maximum between 300 m and 1100 m (up to 3.77 nmol L^{-1}) and rather similar dFe concentrations above and below (~ 1.5 nmol L^{-1}) of this feature. Dissolved Fe showed an approximately linear relationship with nitrate and phosphate (Figure 3). The slope of the regression line was steeper for the offshore stations 2 and 3 than for the two shelf stations 4 and 5.

δ^{56}Fe values for dFe ranged between -0.33 and +0.41 ‰ (Figure 4 and Table 1). δ^{56}Fe values were lowest over the shelf (~ -0.3 ‰) close to the seafloor, and increased towards the crustal value (+0.09 ± 0.10 ‰, 2 SD; Beard et al., 2003) higher up in the water column (Figure 4 and Table 1).

On the slope, Station 3 (1041 m water depth) displayed lowest δ^{56}Fe values (between -0.27 and -0.15 ‰) in oxygen depleted waters. Higher δ^{56}Fe values are observed at 200 m (+0.06 ‰) and 600 m depth (-0.08 ‰). The highest δ^{56}Fe values (-0.06 to +0.41 ‰) were observed at the furthest offshore Station 2 (2656 m water depth). Here, δ^{56}Fe values increased from -0.06 ‰ at 200 m depth to +0.41 ‰ at 500 m depth. Between 600 m and the seafloor, there was little variation in δ^{56}Fe, with values around +0.1 ‰.

4. Discussion

4.1 Benthic supply of dFe

It is now clear, however, that shelf sediments are a source of dFe to overlying seawater even if this water is oxygen replete (Klar et al., 2017a; Mackey et al., 2002; Marsay et al., 2014; Planquette et al., 2007). Thus, the consideration of benthic Fe supply to seawater in biogeochemical models leads to an improved reproduction of dFe distributions (Siedlecki et al., 2012; Tagliabue et al., 2017). The release of dFe from seafloor sediments can be broadly classified into two categories: (i) dissimilatory iron reduction and (ii) non-reductive dissolution.

Dissimilatory iron reduction (DIR) occurs in anoxic sediments and results in the release of soluble Fe(II) into pore waters (e.g., (Severmann et al., 2006), yielding high Fe(II) concentrations in the millimolar range, characterised by a light isotopic signature (-2 to -1 ‰) (Henkel et al., 2016; Homoky et al., 2009; Klar et al., 2017a; Severmann et al., 2006). Upward diffusion of Fe(II) into oxygenated pore waters or overlying bottom water is readily oxidised to Fe(III) (Millero et al., 1987), which forms insoluble amorphous Fe-(oxy)hydroxide minerals at seawater pH (Liu and Millero, 2002; Ussher et al., 2004). It has been observed that as Fe(III) is removed from pore waters, the remaining pore water Fe isotopic composition shifts towards lower values (i.e., δ^{56}Fe down to -3.5 ‰; Severmann et al., 2010). This is in agreement with experimental observations, that have shown that equilibrium fractionation between Fe(II) and Fe(III) results in the δ^{56}Fe value of aqueous Fe(III) being up to 3.5 ‰ greater than that of the coexisting aqueous Fe(II) (e.g., Welch et al., 2003), hence, the δ^{56}Fe value of dFe depends on the proportion of Fe(III) removed from the dissolved phase (Klar et al., 2017b).

On the other hand, non-reductive dissolution (NRD) of lithogenic material leads to the release of dFe with heavier isotopic compositions ($\Delta^{56}Fe_{dFe\text{-}pFe}$ = +0.20 ± 0.11 ‰; Radic et al., 2011), resulting in observed average δ^{56}Fe values of +0.22 ‰ in oxic sediment pore waters (Homoky et al., 2013) and +0.37 ‰ in seawater (Radic et al., 2011). However, benthic Fe fluxes associated with NRD are significantly lower (0.11 to 0.23 µmol Fe m^{-2} d^{-1}; Homoky et al., 2013) than those associated with reductive dissolution in low bottom-water oxygen environments (400 to 866 µmol Fe m^{-2} d^{-1}; Noffke et al., 2012; Severmann et al., 2010).

On the Senegalese shelf, elevated dFe concentrations (up to 6.35 nmol L^{-1}) close to the seafloor are thus indicative of a sedimentary Fe source to the overlying waters. Benthic inputs to the West African margin were also observed on the Mauritanian shelf, at ~18 °N, where diffusive Fe(II) fluxes from shelf sediments (<200 m depth) to bottom waters with <50 µmol kg^{-1} oxygen, determined from pore water Fe concentrations, were between 10 and 30 µmol m^{-2} d^{-1} (Lomnitz, 2017). These fluxes were somewhat lower than fluxes observed on the Californian shelf (<10 to >300 µmol m^{-2} d^{-1}) using

benthic chambers (Severmann et al., 2010). Maximum pore water Fe concentrations were considerably lower (up to 20 µmol L^{-1}) on the Mauritanian shelf than on the Californian margin (up to 300 µmol L^{-1}), indicating that Fe fluxes supplied from sediments are lower on the West African shelf.

Shelf stations 4 and 5 were characterised by low δ^{56}Fe values (down to -0.33 ‰) in low oxygen waters (~50 – 100 µmol kg^{-1}) close to the seafloor (Figure 4). Note that no samples were collected within 50 m of the seafloor at Station 5, so even lower δ^{56}Fe and O_2 values may have been found there. Previous studies (e.g., John et al., 2012; Klar et al., 2017a) have shown that low δ^{56}Fe values indicate pore water Fe(II) efflux to bottom waters. However, even lower δ^{56}Fe values (e.g., down to -3.45 ‰; John et al., 2012) than those reported here have been observed in bottom waters overlying highly reducing margins. Hence, the isotopic composition observed in bottom waters of our study area may reflect the presence of a NRD component. Reported NRD fluxes from marine sediments are insignificant compared to fluxes from DIR. However, reported fluxes from NRD are from regions with a low supply of lithogenic material (low atmospheric dust depositions). Due to high atmospheric dust fluxes to our study area, the NRD component may be more significant, and, hence, potentially makes an important contribution to the entire benthic dFe flux. Other processes that could also explain the relatively high bottom water δ^{56}Fe values are explored below.

As a result of the progressive removal of Fe(III)-(oxy)hydroxides towards the sediment-water interface, sediment porewaters generally show lowest isotopic compositions closest to the surface (down to -3.5 ‰; Severmann et al., 2010). If we were to expect a similar process to occur across the sediment-water interface, even lower δ^{56}Fe values should be observed in bottom waters on the Senegalese margin. However, the relatively higher δ^{56}Fe values in bottom waters (-0.33 ‰), suggest that the isotopic composition has been modified during transport across the sediment-seawater interface. Organic ligands most likely favour the heavy Fe isotopes, with the δ^{56}Fe of ligand bound Fe being up to 0.6 ‰ higher than that of the inorganic Fe fraction (Dideriksen et al., 2008; Morgan et al., 2010). The stabilisation of Fe in bottom waters by ligand complexation could partly prevent precipitation of Fe(III)-(oxy)hydroxides, facilitating the transport of pore water Fe into overlying bottom waters (Hioki et al., 2014; Jones et al., 2011). We therefore suggest that some part of the pore water dFe is complexed with organic ligands, which may also be supplied to sediment pore waters during the degradation of organic material. Dissolved Fe stabilisation due to the complexation to organic ligands at the sediment-water interface has also been suggested in previous studies (e.g. (Klar et al., 2017a), where elevated Fe(II) concentrations were observed in oxic bottom waters over the shelf for longer time periods than predicted, and Fe isotopic signals shifted from as low as -3 ‰ in pore waters to up to -0.1 ‰ in bottom waters. Organic complexation of benthic Fe at the sediment-water interface combined with a NRD component could explain the shift towards higher

δ^{56}Fe values (down to -0.3 ‰) compared to values reported for pore waters elsewhere (as low as ~ -3.5 ‰; e.g., Severmann et al., 2010; Klar et al., 2017a).

In contrast to the shallow coastal stations, bottom waters at slope Station 3 were more oxygenated (up to 140 µmol kg^{-1}), but had similar δ^{56}Fe values (~ -0.3 ‰), suggesting a similar Fe supply mechanism than on the shelf. However, bottom water dFe concentrations (up to 2.9 nmol L^{-1}) were significantly lower at Station 3 compared to stations 4 and 5. Hence, benthic inputs occurred on the slope at Station 3, but were weaker than on the shelf. Elevated dFe concentrations and the benthic Fe isotopic signature (<-0.2 ‰) also persisted ~ 800 m above the seafloor in low oxygen waters at Station 3 (Figure 4), which could be due to upwelling, that is usually high at this time of year (Schott et al., 2004). This is confirmed by the upwards vertical flux of dFe at the bottom of the surface mixed layer at Station 3, that was 0.024 µmol m^{-2} d^{-1} at the time of our study (Milne et al., 2017).

In addition to Fe-ligand complexation, the transport of dFe from sediment pore waters towards the overlying bottom waters and vertical/horizontal transport away from bottom waters may have also been facilitated by low oxygen concentrations (> 45 µmol kg^{-1}; Figure 4) through impediment of Fe(II) removal. Here we assume that sediments are a source of reduced Fe. Although we have no measurements of Fe(II) in our samples, Pacific Ocean waters with oxygen concentrations down to 50 µmol kg^{-1}, contained Fe(II) representing up to 20 % of the dFe pool (Chever et al., 2015). The Fe(II) half-life ($t_{1/2}$) in bottom waters at station 4 and 5 was estimated to be ~ 30 to 70 min (using equations from Millero *et al*., 1987, and [O_2] = 79 to 93 µmol kg^{-1}, T = 16 to 17 °C, Sal = 35.62 to 35.67, pH = 7.75 to 7.80). Theoretical oxidation rates were slower in bottom waters at Station 3, with Fe(II) $t_{1/2}$ ~ 325 min ([O_2] = 130 µmol kg^{-1}, T = 5.4 °C, Sal = 34.84, pH = 7.81). Longer Fe(II) $t_{1/2}$ at this station may have maintained the relatively high dFe concentrations supplied by sediment pore waters, and perhaps partly prevented the formation of Fe-(oxy)hydroxides. Relatively high dFe concentrations within the OMZ on the slope also suggest that longer Fe(II) $t_{1/2}$ may have an effect on the transport of dFe away from bottom waters. However, isotopic compositions characteristic of benthic inputs (<-0.20 ‰ from 400 to 900 m depth) are only observed in the OMZ at Station 3 and not at Station 2 (Figure 4). These findings will be discussed in more detail in Section 4.5.

Negative seawater δ^{56}Fe values attributed to the release of Fe(II) from anoxic sediments into the overlying water column have also been observed in an anoxic basin off the coast of southern California (John et al., 2012). Dissolved Fe concentrations were as high as 29 nmol L^{-1}, δ^{56}Fe values in bottom waters were as low as -3.45 ‰, and bottom water oxygen concentrations were < 5 µmol kg^{-1}. At oxygen concentrations similar to those found within the OMZ in our study (~ 50 to 75 µmol kg^{-1}), dFe in their study ranged from 2.4 to 4.3 nmol L^{-1} and δ^{56}Fe ranged from -1.13 to -0.8 ‰ off the

Californian coast. This suggests that benthic fluxes of dFe are greater in the southern California basin than on the West African margin. In addition, bottom waters in the Peru upwelling area had δ^{56}Fe values as low as -1.25 ‰, associated with O_2 concentrations of < 35 µmol kg^{-1} (Chever et al., 2015; John et al., 2017). These results are in agreement to our findings, considering that the OMZ in the equatorial Pacific Ocean has lower oxygen concentrations than the OMZ in the tropical Atlantic (Stramma et al., 2008b). In addition, Chever et al. (2015) have demonstrated that the dFe pool reflects the isotopic composition of the ferrous Fe, which is presumably released from the sediments. Interestingly, the δ^{56}Fe values of bottom waters on the West African margin were similar to those found in bottom waters of an oxic temperate shelf (-1.0 to -0.1 ‰; Klar et al., 2017a).

Furthermore, our results agree well to low δ^{56}Fe values of down to -0.5 ‰ in the eastern tropical North Atlantic Ocean north of Cape Verde Islands, which were also attributed to Fe released from reducing sediments into a water column with oxygen levels >220 µmol kg^{-1} (Conway and John, 2014). In their study, the shallowest station close to the African shelf was ~ 3000 m deep, hence lacking δ^{56}Fe values on the continental slope and shelf that may have provided further evidence for tracing benthic Fe released into the water column. Our stations, located ~ 6° to the south of the stations shown in Conway and John (2014) complement this coastal gap of δ^{56}Fe values. Conway and John (2014) attributed the end-member δ^{56}Fe value of -2.4 ‰ (observed on the Californian margin, John et al., 2012) to the reducing benthic Fe source from the eastern margin for calculating its contribution to their ocean transect. However, our study suggests that the end-member δ^{56}Fe value of the reducing benthic Fe source may be closer to -0.3 ‰ on the eastern tropical North Atlantic margin, which would allow for a better constrained estimation of its inputs to the ocean. Nevertheless, we also advise that mass-balance calculations using Fe isotopes should be used with caution due to the reactive nature of Fe in seawater, which is mostly associated with isotopic fractionation.

The eastern tropical Atlantic is characterised by relatively high upwelling rates (e.g., Ussher et al., 2013), and therefore high dFe bottom waters are most likely transported towards surface waters, especially on the shelf. Shelf and slope waters loaded with dFe were most likely advected along isopycnals towards the open ocean due to the westward direction of the main currents in this area. This is confirmed by net upwards vertical fluxes below the surface mixed layer and net offshore horizontal fluxes that were calculated in our study area (Milne et al., 2017). Horizontal dFe fluxes were highest on the shelf (5185 µmol m^{-2} d^{-1}) and decreased with distance from the coast (down to 21.5 µmol m^{-2} d^{-1} at Station 2; Milne et al., 2017). Vertical upward dFe fluxes were also highest on the shelf (16 µmol m^{-2} d^{-1} *vs* 0.024 to 0.043 on the slope).

4.2 Atmospheric supply of Fe to the surface ocean

The study area is located in close proximity to the Sahara and Sahel deserts, which deliver large amounts of dust to the North Atlantic Ocean (Jickells et al., 2005; Kramer et al., 2004; Patey et al., 2015). Dissolved aluminium (dAl) is a near conservative tracer of lithogenic material in seawater (Measures and Brown, 1996), as it is only removed by scavenging processes (Moran and Moore, 1992) with minor incorporation into siliceous frustules (Gehlen et al., 2002). Assuming that dAl in the surface mixed layer is entirely supplied by atmospheric dust, that dust is composed of 8.2 % w/w Al and 5.6 % w/w Fe (Taylor, 1964), and that both elements are dissolved in the same proportion, dust supplied dFe can be calculated (Table 2). Accordingly, 60 % of dFe in the surface mixed layer is provided by dust on the shelf and 50 to 155 % on the slope. Some part of the Fe supplied to the surface mixed layer may have been taken up by phytoplankton or scavenged onto sinking particles. This may explain why we observe lower dFe concentrations at Station 3 than calculated from dAl concentrations. At the other stations, the excess dFe may have been supplied from shelf sediments and were upwelled. Assuming that the residence time of dAl is 1.2 ± 0.5 years in tropical Atlantic waters (Dammshäuser et al., 2011), and that 4 ± 2 % of Saharan dust is dissolved in seawater (Buck et al., 2010), the aerosol dFe flux is estimated to be 0.17 ± 0.14 µmol m^{-2} d^{-1} on the shelf and 0.20 – 0.71 µmol m^{-2} d^{-1} on the slope (Table 2).

This compares well with direct aerosol measurements and soluble aerosol Fe flux estimates performed during the same cruise. The soluble Fe flux from aerosols was 0.075 µmol m^{-2} d^{-1} on the shelf (Stations 4 and 5) and 0.074 µmol m^{-2} d^{-1} on the slope, compared to 0.135 µmol m^{-2} d^{-1} in the open ocean at 12 °N (Milne et al., 2017). Slight differences between the methods are expected, as aerosol fluxes derived from dAl measurements in surface waters represent average fluxes over ~ 1.2 years. It should be noted that the aerosol flux calculation from Al is linked to major caveats and assumptions. Al is highly particle reactive and, hence, its concentration in surface waters is most likely influenced by particle loading (Figure 4). Therefore, the aerosol fluxes calculated from dAl concentrations are highly dependent on Al residence times, which are controlled by particle scavenging. Aerosol fluxes can be as high as 74 µmol Fe m^{-2} d^{-1} on the West African margin during dust storms (Croot et al., 2004). Hence, atmospheric depositions were relatively low but significant in our study area at the time of sampling.

We have no δ^{56}Fe measurements from within the surface mixed layer (SML, 11 to 19 m thick) and dFe isotopic compositions are likely significantly modified below the SML due to scavenging and remineralisation processes. Hence, we are not able to assess the isotopic composition of dust-derived dFe in our study area. However, surface waters at 25 m depth on the shelf were characterised by higher δ^{56}Fe values (-0.11 to +0.03 ‰), and lower dFe concentrations (up to 3 nmol

L^{-1}), compared to bottom waters (Figure 4). The shift towards higher isotopic values from 40 towards 25 m depth is indicative of dust-derived dFe to the surface ocean. NRD of sinking lithogenic material leads to the release of dFe with high $\delta^{56}Fe$ values +0.27 ± 0.25 ‰ higher (Labatut et al., 2014) than that of the lithogenic material ($\delta^{56}Fe$ ~ +0.07 ± 0.11 ‰; Mead et al., 2013; Waeles et al., 2007). Hence, NRD may explain the relatively high $\delta^{56}Fe$ values throughout the water column on the shelf. In the North Atlantic Ocean, north of Cape Verde islands, high $\delta^{56}Fe$ values of +0.3 to +0.7 ‰ in the surface mixed layer were attributed to a strong atmospheric dust supply (Conway and John, 2014). The high $\delta^{56}Fe$ values of the aerosol signal in seawater, relative to that of atmospheric dust ($\delta^{56}Fe$ ~ +0.07 ± 0.11 ‰; Mead et al., 2013; Waeles et al., 2007) was attributed to the formation of strong Fe-ligand complexes during dust dissolution, which preferentially incorporate the heavier Fe isotopes ($\Delta^{56}Fe_{LFe\text{-}dFe}$ = 0.6 ‰; (Dideriksen et al., 2008; Morgan et al., 2010). To properly asses the effects of atmospheric deposition on the isotopic composition of dFe in seawater, we are lacking isotopic measurements of aerosols in the study area and of particulate material in the water column.

4.3 Fe Isotopic fractionation by biogeochemical processes

Concentrations of chlorophyll-a indicated that levels of biological activity in the surface waters were high, with levels up to ~1.5 µg L^{-1} on the shelf and up to 2 µg L^{-1} on the slope (Figure 4). Maximum Chl-a and lowest transmittance were immediately below the surface layer (0 to 15 m depth) and thus above the shallowest Fe isotopes sample. It is important to note that significant changes in $\delta^{56}Fe$ values linked to high biological activity are expected in surface waters. Uptake of isotopically light Fe linked to biological activity has previously been observed ($\Delta^{56}Fe_{PFe\text{-}DFe}$ < -0.54 ‰; Ellwood et al., 2015; Radic et al., 2011). By contrast, (Conway and John, 2014) record relatively light $\delta^{56}Fe$ values of dFe (e.g., -0.01 ‰ vs +0.20 ‰ above and below) associated with the deep fluorescence maximum (136 m) in the North Atlantic Ocean. John et al. (2017) observed a decrease in $\delta^{56}Fe$ of dFe in the upper few hundred metres and suggested this to be due to biological uptake, however, this was not observed in all their profiles. The direction of Fe isotopic fractionation could depend on phytoplankton type.

Even though we were not able to assess the isotopic fractionation of Fe associated with biological uptake directly, we were able to do this indirectly by investigating remineralisation of sinking organic material throughout the water column. Remineralisation of sinking organic material plays an important role in recycling Fe in the ocean (e.g., Fitzsimmons et al., 2013; Rijkenberg et al., 2012). The amount of remineralised dFe in the water column was calculated from apparent oxygen utilisation (AOU), assuming an AOU/C ratio of 1.6 (Martin et al., 1987) and a Fe/C ratio of 15 µmol Fe/mol C, measured in phytoplankton cells on the west African margin (Twining et al., 2015) (Figure 5). This ratio is similar to that estimated in the eastern tropical North Atlantic during cruise AMT15

(13 µmol Fe/mol C; Ussher et al. (2013)). These calculations suggest that on the shelf, 25 to 40 % of dFe was provided by remineralisation of sinking organic material. The rest must have been supplied by another source, most likely sediments. On the slope at Station 2, remineralisation was the dominant dFe source, especially within the OMZ (between 40 and 900 m depth), and partly represented > 100 % dFe, which suggests that part of the remineralised dFe had been rapidly removed by scavenging processes.

Higher levels of remineralisation were associated with the release of relatively heavy Fe isotopes (Figure 5). It has been shown that remineralisation of organic material is less effective in OMZs (Cavan et al., 2017), and therefore, it is not certain if the high δ^{56}Fe values are reflecting the remineralisation of the entire biogenic Fe pool or that of an unknown fraction. Other processes such as adsorption/desorption of Fe onto/from particles and dissolution of lithogenic particles could overprint δ^{56}Fe values throughout the water column, however, we suggest that these changes are relatively small. At Station 3, highest remineralisation extents at 600 m depth (Figure 5) coincided with a δ^{56}Fe value of -0.08 ‰. At Station 2, the proportion of dFe supplied by remineralisation was consistently highest within the OMZ and was correlated to high δ^{56}Fe values (+0.02 to +0.41 ‰). Highest remineralisation proportions at Station 2 coincided with a δ^{56}Fe value of +0.41 ‰ at 500 m depth, the highest δ^{56}Fe value measured in this study. Interestingly, these relatively high isotopic values were associated with a decrease in dFe concentrations at both stations, suggesting rapid scavenging onto particles. Therefore, scavenging of dFe onto particles could also explain the heavy isotopic compositions. Our results suggest biological uptake of heavy dFe isotopes in surface waters, followed by release of heavy dFe isotopes during remineralisation of this material as it sinks throughout the water column followed by rapid scavenging of some part of the remineralised dFe onto sinking particles. Our results contradict previous studies, which suggested that biological Fe uptake incorporates the lighter isotopes (Ellwood et al., 2015; Radic et al., 2011). However, our results are consistent with the findings in Conway et al (2014), where isotopically light dFe was associated with the deep fluorescence maxima and the dFe concentration minima in the North Atlantic.

The nearly constant dFe concentrations (1.3 to 1.7 nmol L^{-1}) below 1400 m depth at Station 2, associated with constant δ^{56}Fe values (~+0.1 ‰) may be the result of a dynamic exchange of Fe between the dissolved and particulate phases (Homoky et al., 2012; John and Adkins, 2012; Labatut et al., 2014; Milne et al., 2017). The combination of the different processes involving particles, that include scavenging of Fe onto particles, desorption and non-reductive dissolution from sinking lithogenic particles, potentially leads to dFe isotopic fractionation observed (Abadie et al., 2017; Ellwood et al., 2015; John and Adkins, 2012; John et al., 2017).

4.4 Isotopic signatures within water masses

Between 700 and 1100 m water depth, AAIW was present at stations 2 and 3. The δ^{56}Fe values in this water mass were ~ +0.1 ‰ (*n = 3*) at Station 2 and -0.30 to -0.08 ‰ (*n = 4*) at Station 3. AAIW was located immediately over the seafloor at Station 3, with enhanced dFe concentrations and low δ^{56}Fe values indicating a relatively strong supply of benthic dFe to bottom waters, overwriting the isotopic signature of AAIW. In previous studies, it has been observed that AAIW transports isotopically light Fe (-0.37 to -0.17 ‰) within southern hemisphere basins of the Atlantic and Pacific Oceans (Abadie et al., 2017; Fitzsimmons et al., 2016). The Fe isotopic signature of AAIW is significantly modified at the equator (+0.22 ‰, Radic et al., 2011) and close to Papua New Guinea (+0.06 to +0.44 ‰) (Labatut et al., 2014; Radic et al., 2011). Abadie et al. (2017) observed that the light δ^{56}Fe values may originate from the dilution of Upper Circumpolar Deep Water (UCDW; ~ -0.8 ‰), as AAIW originates from the subduction of Antarctic Surface Water (AASW), which in turn results from the upwelling of UCDW. We suggest that the δ^{56}Fe values we observed in AAIW are significantly modified by remineralisation, sorption/desorption processes and sedimentary supply of new dFe.

At Station 2 NADW was present at depths between 1100 m and the seafloor (2656 m), with a δ^{56}Fe value of +0.09 to +0.12 ‰ (*n = 2*) and dFe concentrations of 1.3 to 1.7 nmol L^{-1}. Reported δ^{56}Fe values for NADW differ significantly in the literature. In the North Atlantic Ocean, Conway and John (2014) reported δ^{56}Fe values of ~ +0.21 ‰ at ~ 2000 m depth for a profile over the continental slope at ~ 18° W, and δ^{56}Fe values of ~ +0.7 ‰ at 2000 m depth at 30° W in the open ocean. Near Bermuda, the δ^{56}Fe of NADW ranged from +0.4 to +0.7 ‰ (John and Adkins, 2012). NADW measured at ~3000 m depth in the Southern Ocean has reported δ^{56}Fe values between +0.2 to +0.3 ‰ (Abadie et al., 2017). This suggests that the isotopic composition of NADW is modified during its southwards journey. Such processes might include: (i) exchange between the dissolved and particulate Fe pools (Ellwood et al., 2015; John and Adkins, 2012; Labatut et al., 2014; Radic et al., 2011), and (ii) non-reductive dissolution of sinking particles (Abadie et al., 2017).

Due to the short residence times and reactivity of Fe, and the supply of new Fe close to source regions, the isotopic composition of the dissolved Fe pool is continuously modified and cannot be applied as a conservative water mass tracer.

4.5 The source of elevated dFe concentrations in low oxygen waters off the shelf

The elevated dFe concentrations observed in the OMZ (between 40 and 900 m depth) at Station 2 may originate from offshore advection of high dFe containing shelf waters (Conway and John, 2014), remineralisation of sinking particles (Fitzsimmons et al., 2013), and the net release of dFe from particle surfaces (Milne et al., 2017). δ^{56}Fe values exhibited a negative correlation with dFe

concentrations, suggesting that most of the isotopic variations observed at our study site can be explained with mixing between high dFe concentration, low δ^{56}Fe shelf waters and low dFe concentration, high δ^{56}Fe offshore water masses (Figure 6a). On the shelf, a positive correlation between oxygen concentrations and δ^{56}Fe values could be an artefact due to larger amounts of oxygen being consumed in deeper waters combined with poor ventilation indicates that redox processes might have been dominating the dFe isotopic signatures (Figure 6b). However, this good correlation disappeared on the slope, which suggests that elevated dFe concentrations were not solely linked to low oxygen concentrations in waters off the shelf. We cannot assume that isotopic signatures are solely governed by mixing processes, and hence, explore other possibilities below.

We have estimated the amount of dFe released to the water column due to remineralisation processes, and this was up to 2.1 nmol L^{-1} within low oxygen waters on the slope (Figure 5; section 4.3). The contribution of remineralisation to the dFe concentrations measured in low oxygen waters was 25 to 40 % (average 33 ± 5, *n = 10*) on the shelf, 56 to 170 % (average 88 ± 36 %, *n = 11*) at Station 3 and 94 to 150 % (average 118 ± 22, *n = 9*) at Station 2. Hence, the importance of remineralised dFe increased with distance from the shelf. The AOU was positively correlated with dFe concentrations in all profiles, where shelf and slope stations lie on different slopes, which could be a result of different phytoplankton community structures that have different Fe requirements between these regions (Figure 7a). Highest remineralisation dFe contributions were correlated to highest δ^{56}Fe values on the slope (Figure 7b). Hence, the high δ^{56}Fe values (-0.06 to 0.41 ‰, average +0.1 ± 0.3 ‰, *n = 7*) observed in oxygen low waters at Station 2 were mainly provided through remineralisation of sinking organic matter.

"Excess" dFe (dFe supplied from processes other than remineralisation) is highest on the shelf (Figure 5) and correlates with low δ^{56}Fe values on the slope (Figure 7b). Due to the overall association to low δ^{56}Fe values, excess dFe can be mainly attributed to benthic inputs from sediments. However, it is evident that excess dFe was composed of additional sources, as well as benthic sources, on the shelf because excess dFe correlates with higher (instead of lower) δ^{56}Fe values (Figure 7b). The higher δ^{56}Fe values on the shelf were most likely due to the presence of aerosol inputs and increased NRD of lithogenic material towards the surface ocean (as discussed in section 4.2). On the shelf, the excess dFe was 2.4 ± 0.8 nmol L^{-1} *(n = 10*) with a maxima at 4.7 nmol L^{-1}, which represented as much as 75 % of dFe supplied to the water column by processes other than remineralisation. This is also where lowest δ^{56}Fe values (-0.33 to -0.20 ‰) were observed below 40 m depth (Figure 4), indicative of a strong benthic dFe source. On the slope, an average of 0.6 ± 0.7 nmol L^{-1} dFe (*n = 11*) and up to 1.6 nmol L^{-1} at 500 and 800 m depth could have been supplied by benthic inputs to low oxygen waters at Station 3. Where excess dFe was highest at Station 3, δ^{56}Fe values

were also lowest (as low as -0.32 ‰ at 500 m depth), indicating a benthic source. At Station 2, there was generally no excess dFe within low oxygen waters, so relatively high dFe concentrations are associated with remineralisation. A small excess dFe concentration (0.12 nmol L^{-1}) at 200 m depth was associated with a lower δ^{56}Fe value (-0.06 ‰), which can be attributed to a dilute benthic influence at Station 2.

Scavenging of dFe onto biogenic and non-biogenic particles and exchange of Fe between the dissolved and particulate phases are continuous processes within the water column and are likely to overprint the isotopic signatures of benthic/atmospheric inputs and remineralisation. However, we are not able to assess the effects of these processes in this study and assume that the associated isotopic fractionation was small (Ellwood et al., 2015; Labatut et al., 2014; Radic et al., 2011).

Benthic dFe inputs from shelf and slope sediments and, to a lower extent at the time of our study, atmospheric dFe inputs therefore appear to make an important contribution to the supply of "new" dFe to the study area. We observe that waters containing high dFe concentrations and light isotopic compositions are transported off the shelf to the slope region, which could be facilitated by the westward flowing NECC and the nNECC. This assumption is confirmed by relatively high horizontal dFe fluxes below the SML on the shelf (5185 µmol dFe m^{-2} d^{-1}) and slope (94.4 µmol dFe m^{-2} d^{-1} at Station 3) regions (Figure 8; Milne et al., 2017). The benthic isotopic signal of dFe is considerably weakened at Station 2, as is the horizontal flux (21.5 µmol dFe m^{-2} d^{-1} at Station 2 ;Milne et al., 2017), ~37 km from the shelf stations. Likewise, remineralisation processes gain importance in the supply of dFe to the OMZ with distance from the shelf. We suggest that a considerable proportion of the recycled dFe is initially sourced from benthic and (to a minor degree at the time of sampling) atmospheric inputs in our study area. Here we observed a snapshot of what could be the repetition of continuous cycles of upwelling of high dFe bottom waters, followed by biological uptake, particle sinking and remineralisation (followed by upwelling, etc), which leads to a net shift towards heavier dFe isotopic compositions of the initially isotopically light benthic signal within the OMZ as moving offshore (Figure 8). We envision that a significant part of sinking organic material is not remineralised within the OMZ and is exported towards deeper waters, because remineralisation rates may be low in OMZs (Cavan et al., 2017). Hence, the supply of new Fe (benthic and atmospheric) must play an important role in maintaining the high Fe concentrations in the tropical North Atlantic OMZ.

Our results confirm previous studies of dFe concentrations, that inferred that remineralisation plays a key role in the supply of dFe to the subsurface waters of offshore regions of the tropical Atlantic OMZ (Fitzsimmons et al., 2013; Rijkenberg et al., 2012). These studies observed a near constant slope between dFe and AOU, that indicated that the main dFe source was from remineralisation from

sinking material with a fixed Fe:C ratio. Rijkenberg et al. (2012) observed a shift to higher Fe:C ratios north of 25 °N, indicative of external sources, which were attributed to shelf inputs.

Our results are partly consistent with a study north of Cape Verde islands that suggest that a shelf signal may be observed up to 1000 km outside the OMZ in the open ocean (with O_2 > 160 µmol kg^{-1}) (Conway and John, 2014). They suggest that 20 to 30 % of the dFe found in the water column on the continental margins originates from reductive sediments. However, Conway and John (2014) selected the δ^{56}Fe value of -2.4 ‰ from the Californian margin (John et al., 2012) as the benthic dFe endmember to calculate its contribution to the entire ocean section. Our study indicates that the δ^{56}Fe value of benthic supplied dFe must be closer to -0.3 ‰ on the eastern tropical Atlantic margin. However, here we demonstrate that remineralisation processes can overprint dFe advected from the shelf considerably, hence mass balance calculations using Fe isotopes should be applied with caution.

5. Conclusions

Our study confirms that remineralisation plays an important role in recycling Fe within the tropical North Atlantic OMZ, but, in contrast to previous work, we provide evidence of significant benthic dFe inputs to low oxygen waters. At times of low atmospheric dust depositions, we suggest that “new” Fe is initially supplied by benthic inputs, and that consecutive cycles of bottom water upwelling, biological uptake, and remineralisation of sinking of organic matter lead to the enhanced dFe concentrations observed in the eastern boundary tropical North Atlantic OMZ. We also suggest that benthic supplied dFe must be stabilised by complexation to organic ligands.

It is certain that regeneration of sinking organic material from the highly productive surface ocean is key in maintaining high dFe concentrations within the tropical Atlantic OMZ, and that upwelling can act as a transport vector to the surface ocean. Atmospheric dust deposition was low during the time of our study but is known to be highly variable. The relative importance of new Fe provided from atmospheric versus benthic Fe inputs to the surface ocean of the tropical North Atlantic as an annual mean remains uncertain.

Because oxygen concentrations in seawater may have an influence on remineralisation rates and Fe speciation, the decline in oxygen concentrations due to global warming may have significant consequences on Fe cycling. This needs to be investigated and incorporated into future modelling efforts of the linkages between biogeochemical cycles and climate.

6. Acknowledgements

We gratefully acknowledge the support of the captain and crew of *RRS Discovery* throughout cruise D361. We also thank NMF staff for their technical assistance on-board. We thank the rest of the trace metal sampling team Maeve C Lohan, Angela Milne and Felix Morales for their hard work on-board. We thank Eithne Tynan for pH data and Alexander Forryan for help with CTD data.

7. Funding

This study was funded by the UK National Environmental Research Council (NE/G015732/1) and the Atlantic Meridional Transect consortium (243). JKK's PhD studentship was funded by the Graduate School of the National Oceanography Centre and NERC National Capability Funds.

8. List of tables

9. List of figures

Figure 4: Profiles of Chl-a, transmittance, oxygen concentrations, dFe concentrations and δ^{56}Fe values at a) slope stations 2 and 3 and b) shelf stations 4 and 5. dFe data are from (Milne et al., 2017). Note change of scale for dFe concentrations between upper and lower plots. The average δ^{56}Fe value of the continental crust is shown as a vertical black line (+0.09 ± 0.10 ‰, 2 SD, *n = 46*; Beard et al., 2003).

Figure 5: Proportions of calculated remineralised dFe concentrations, relative to measured dFe concentrations (a) on the shelf and (b) on the slope.

Figure 6: Relationship of (a) δ^{56}Fe *vs* dFe; and (b) δ^{56}Fe *vs* O_2 on the shelf (stations 4 and 5) and on the slope (stations 2 and 3). The average δ^{56}Fe value of the continental crust (+0.09 ± 0.10 ‰; Beard et al., 2003) is shown with black lines. Linear regressions of the δ^{56}Fe *vs* dFe relationship for the entire data set and of the δ^{56}Fe *vs* O_2 on the shelf are shown with dotted lines and their equations are displayed.

Figure 7: (a) Relationship between dFe and AOU in the upper 1000 m of the water column and (b) relationship between δ^{56}Fe and remineralised dFe (dFe_{remin}) for the shelf (stations 4 and 5) and the slope (stations 2 and 3) regions. The average δ^{56}Fe value of the continental crust (+0.09 ± 0.10 ‰; Beard et al., 2003) is shown with a black line in (b). Linear regressions are shown with dotted lines and their equations are displayed.

Figure 8: Simplified view of the Fe cycle in our study area. Shelf sediments supply dFe with a light isotopic composition (↓ δ^{56}Fe) to bottom waters. dFe is supplied to the surface mixed layer (SML) by atmospheric dust deposition and upwelled bottom waters, where phytoplankton takes up dFe with a relatively heavy isotopic composition (↑ δ^{56}Fe). Remineralisation of sinking organic material leads to the release of dFe with a relatively heavy isotopic composition, which is mixed with benthic dFe inputs and upwelled to the SML, where it is mixed with atmospheric dFe inputs. The flux of benthic dFe decreases with distance from the coast. The continuous recycling of dFe by biological uptake and remineralisation leads to increasingly heavy isotopic compositions of dFe in the water column moving offshore. Atmospheric dust inputs (fluxes in µmol dFe m^{-2} d^{-1}, in brown) to the SML, calculated from dAl concentrations, were low at the time of sampling but are potentially higher at other times of the year (Croot et al., 2004). Fluxes of vertical transport to the SML (white) and horizontal transport between the bottom of the SML and 500 m depth (yellow) are from Milne et al. (2017) and are in µmol dFe m^{-2} d^{-1}.

10. References

Abadie, C., Lacan, F., Radic, A., Pradoux, C. and Poitrasson, F. (2017) Iron isotopes reveal distinct dissolved iron sources and pathways in the intermediate versus deep Southern Ocean. Proceedings of the National Academy of Sciences 114, 858-863.

Beard, B.L., Johnson, C.M., Von Damm, K.L. and Poulson, R.L. (2003) Iron isotope constraints on Fe cycling and mass balance in oxygenated Earth oceans. Geology 31, 629-632.

Bergquist, B.A. and Boyle, E.A. (2006) Iron isotopes in the Amazon River system: Weathering and transport signatures. Earth. Planet. Sci. Lett. 248, 54-68.

Berman-Frank, I., Cullen, J.T., Shaked, Y., Sherrell, R.M. and Falkowski, P.G. (2001) Iron availability, cellular iron quotas, and nitrogen fixation in Trichodesmium. Limnol. Oceanogr. 46, 1249-1260.

Boyd, P.W. and Ellwood, M.J. (2010) The biogeochemical cycle of iron in the ocean. Nat. Geosci. 3.

Boyle, E.A., John, S., Abouchami, W., Adkins, J.F., Echegoyen-Sanz, Y., Ellwood, M., Flegal, A.R., Fornace, K., Gallon, C., Galer, S., Gault-Ringold, M., Lacan, F., Radic, A., Rehkamper, M., Rouxel, O., Sohrin, Y., Stirling, C., Thompson, C., Vance, D., Xue, Z. and Zhao, Y. (2012) GEOTRACES IC1 (BATS) contamination-prone trace element isotopes Cd, Fe, Pb, Zn, Cu, and Mo intercalibration. Limnol. Oceanogr. Meth. 10, 653-665.

Brandt, P., Hormann, V., Kortzinger, A., Visbeck, M., Krahmann, G., Stramma, L., Lumpkin, R. and Schmid, C. (2010) Changes in the Ventilation of the Oxygen Minimum Zone of the Tropical North Atlantic. J. Phys. Oceanogr. 40, 1784-1801.

Brown, M.T. and Bruland, K.W. (2008) An improved flow-injection analysis method for the determination of dissolved aluminum in seawater. Limnol. Oceanogr. Meth. 6, 87-95.

Buck, C.S., Landing, W.M., Resing, J.A. and Measures, C.I. (2010) The solubility and deposition of aerosol Fe and other trace elements in the North Atlantic Ocean: Observations from the A16N CLIVAR/CO(2) repeat hydrography section. Mar. Chem. 120, 57-70.

Cavan, E.L., Trimmer, M., Shelley, F. and Sanders, R. (2017) Remineralization of particulate organic carbon in an ocean oxygen minimum zone. 8, 14847.

Chan, F., Barth, J.A., Lubchenco, J., Kirincich, A., Weeks, H., Peterson, W.T. and Menge, B.A. (2008) Emergence of anoxia in the California current large marine ecosystem. Science 319, 920-920.

Chever, F., Rouxel, O.J., Croot, P.L., Ponzevera, E., Wuttig, K. and Auro, M. (2015) Total dissolvable and dissolved iron isotopes in the water column of the Peru upwelling regime. Geochim. Cosmochim. Acta 162, 66-82.

Coale, K.H., Johnson, K.S., Chavez, F.P., Buesseler, K.O., Barber, R.T., Brzezinski, M.A., Cochlan, W.P., Millero, F.J., Falkowski, P.G., Bauer, J.E., Wanninkhof, R.H., Kudela, R.M., Altabet, M.A., Hales, B.E., Takahashi, T., Landry, M.R., Bidigare, R.R., Wang, X.J., Chase, Z., Strutton, P.G., Friederich, G.E., Gorbunov, M.Y., Lance, V.P., Hilting, A.K., Hiscock, M.R., Demarest, M., Hiscock, W.T., Sullivan, K.F., Tanner, S.J., Gordon, R.M., Hunter, C.N., Elrod, V.A., Fitzwater, S.E., Jones, J.L., Tozzi, S., Koblizek, M., Roberts, A.E., Herndon, J., Brewster, J., Ladizinsky, N., Smith, G., Cooper, D., Timothy, D., Brown, S.L., Selph, K.E., Sheridan, C.C., Twining, B.S. and Johnson, Z.I. (2004) Southern ocean iron enrichment experiment: Carbon cycling in high- and low-Si waters. Science 304, 408-414.

Conway, T.M. and John, S.G. (2014) Quantification of dissolved iron sources to the North Atlantic Ocean. Nature advance online publication.

Croot, P.L., Streu, P. and Baker, A.R. (2004) Short residence time for iron in surface seawater impacted by atmospheric dry deposition from Saharan dust events. Geophysical Research Letters 31, L23S08.

Dammshäuser, A., Wagener, T. and Croot, P.L. (2011) Surface water dissolved aluminum and titanium: Tracers for specific time scales of dust deposition to the Atlantic? Geophysical Research Letters 38.

Dideriksen, K., Baker, J.A. and Stipp, S.L.S. (2008) Equilibrium Fe isotope fractionation between inorganic aqueous Fe(III) and the siderophore complex, Fe(III)-desferrioxamine B. Earth. Planet. Sci. Lett. 269, 280-290.

Ellwood, M.J., Hutchins, D.A., Lohan, M.C., Milne, A., Nasemann, P., Nodder, S.D., Sander, S.G., Strzepek, R., Wilhelm, S.W. and Boyd, P.W. (2015) Iron stable isotopes track pelagic iron cycling during a subtropical phytoplankton bloom. Proceedings of the National Academy of Sciences 112, E15-E20.

Escoube, R., Rouxel, O.J., Sholkovitz, E. and Donard, O.F.X. (2009) Iron isotope systematics in estuaries: The case of North River, Massachusetts (USA). Geochim. Cosmochim. Acta 73, 4045-4059.

Falkowski, P.G. (1997) Evolution of the nitrogen cycle and its influence on the biological sequestration of CO2 in the ocean. Nature 387, 272-275.

740 Fitzsimmons, J.N., Conway, T.M., Lee, J.M., Kayser, R., Thyng, K.M., John, S.G. and Boyle, E.A.
741 (2016) Dissolved iron and iron isotopes in the southeastern Pacific Ocean. Global Biogeochem. Cycles
742 30, 1372-1395.

743 Fitzsimmons, J.N., Zhang, R. and Boyle, E.A. (2013) Dissolved iron in the tropical North Atlantic
744 Ocean. Mar. Chem. 154, 87-99.

745 Gehlen, M., Beck, L., Calas, G., Flank, A.M., Van Bennekom, A.J. and Van Beusekom, J.E.E.
746 (2002) Unraveling the atomic structure of biogenic silica: Evidence of the structural association of Al
747 and Si in diatom frustules. Geochim. Cosmochim. Acta 66, 1601-1609.

748 Gledhill, M. and Buck, K.N. (2012) The organic complexation of iron in the marine
749 environment: a review. Frontiers in Microbiology 3.

750 Goldberg, E.D. (1954) Marine Geochemistry 1. Chemical Scavengers of the Sea. The Journal of
751 Geology 62, 249-265.

752 Henkel, S., Kasten, S., Poulton, S.W. and Staubwasser, M. (2016) Determination of the stable
753 iron isotopic composition of sequentially leached iron phases in marine sediments. Chem. Geol. 421,
754 93-102.

755 Hioki, N., Kuma, K., Morita, Y., Sasayama, R., Ooki, A., Kondo, Y., Obata, H., Nishioka, J.,
756 Yamashita, Y., Nishino, S., Kikuchi, T. and Aoyama, M. (2014) Laterally spreading iron, humic-like
757 dissolved organic matter and nutrients in cold, dense subsurface water of the Arctic Ocean. 4, 6775.

758 Homoky, W.B., John, S.G., Conway, T.M. and Mills, R.A. (2013) Distinct iron isotopic signatures
759 and supply from marine sediment dissolution. Nat Commun 4.

760 Homoky, W.B., Severmann, S., McManus, J., Berelson, W.M., Riedel, T.E., Statham, P.J. and
761 Mills, R.A. (2012) Dissolved oxygen and suspended particles regulate the benthic flux of iron from
762 continental margins. Mar. Chem. 134, 59-70.

763 Homoky, W.B., Severmann, S., Mills, R.A., Statham, P.J. and Fones, G.R. (2009) Pore-fluid Fe
764 isotopes reflect the extent of benthic Fe redox recycling: Evidence from continental shelf and deep-
765 sea sediments. Geology 37, 751-754.

766 Jickells, T.D., An, Z.S., Andersen, K.K., Baker, A.R., Bergametti, G., Brooks, N., Cao, J.J., Boyd,
767 P.W., Duce, R.A., Hunter, K.A., Kawahata, H., Kubilay, N., laRoche, J., Liss, P.S., Mahowald, N.,
768 Prospero, J.M., Ridgwell, A.J., Tegen, I. and Torres, R. (2005) Global iron connections between desert
769 dust, ocean biogeochemistry, and climate. Science 308, 67-71.

John, S.G. and Adkins, J. (2012) The vertical distribution of iron stable isotopes in the North Atlantic near Bermuda. Global Biogeochem. Cycles 26.

John, S.G. and Adkins, J.F. (2010) Analysis of dissolved iron isotopes in seawater. Mar. Chem. 119, 65-79.

John, S.G., Helgoe, J., Townsend, E., Weber, T., DeVries, T., Tagliabue, A., Moore, K., Lam, P., Marsay, C.M. and Till, C. (2017) Biogeochemical cycling of Fe and Fe stable isotopes in the Eastern Tropical South Pacific. Mar. Chem.

John, S.G., Mendez, J., Moffett, J. and Adkins, J. (2012) The flux of iron and iron isotopes from San Pedro Basin sediments. Geochim. Cosmochim. Acta 93, 14-29.

Jones, M.E., Beckler, J.S. and Taillefert, M. (2011) The flux of soluble organic-iron(III) complexes from sediments represents a source of stable iron(III) to estuarine waters and to the continental shelf. Limnol. Oceanogr. 56, 1811-1823.

Karstensen, J., Stramma, L. and Visbeck, M. (2008) Oxygen minimum zones in the eastern tropical Atlantic and Pacific oceans. Prog. Oceanogr. 77, 331-350.

Keeling, R.F., Koertzinger, A. and Gruber, N. (2010) Ocean Deoxygenation in a Warming World. Annual Review of Marine Science 2, 199-229.

Klar, J.K., Homoky, W.B., Statham, P.J., Birchill, A.J., Harris, E.L., Woodward, E.M.S., Silburn, B., Cooper, M.J., James, R.H., Connelly, D.P., Chever, F., Lichtschlag, A. and Graves, C. (2017a) Stability of dissolved and soluble Fe(II) in shelf sediment pore waters and release to an oxic water column. Biogeochemistry.

Klar, J.K., James, R.H., Gibbs, D., Lough, A., Parkinson, I., Milton, J.A., Hawkes, J.A. and Connelly, D.P. (2017b) Isotopic signature of dissolved iron delivered to the Southern Ocean from hydrothermal vents in the East Scotia Sea. Geology 45, 351-354.

Klunder, M.B., Laan, P., Middag, R., de Baar, H.J.W. and Bakker, K. (2012) Dissolved iron in the Arctic Ocean: Important role of hydrothermal sources, shelf input and scavenging removal. J. Geophys. Res.-Oceans 117.

Klunder, M.B., Laan, P., Middag, R., De Baar, H.J.W. and van Ooijen, J.C. (2011) Dissolved iron in the Southern Ocean (Atlantic sector). Deep Sea Research Part II: Topical Studies in Oceanography 58, 2678-2694.

Kramer, J., Laan, P., Sarthou, G., Timmermans, K.R. and de Baar, H.J.W. (2004) Distribution of dissolved aluminium in the high atmospheric input region of the subtropical waters of the North Atlantic Ocean. Mar. Chem. 88, 85-101.

Labatut, M., Lacan, F., Pradoux, C., Chmeleff, J., Radic, A., Murray, J.W., Poitrasson, F., Johansen, A.M. and Thil, F. (2014) Iron sources and dissolved-particulate interactions in the seawater of the Western Equatorial Pacific, iron isotope perspectives. Global Biogeochem. Cycles 28, 1044-1065.

Lacan, F., Radic, A., Jeandel, C., Poitrasson, F., Sarthou, G., Pradoux, C. and Freydier, R. (2008) Measurement of the isotopic composition of dissolved iron in the open ocean. Geophysical Research Letters 35.

Lacan, F., Radic, A., Labatut, M., Jeandel, C., Poitrasson, F., Sarthou, G., Pradoux, C., Chmeleff, J. and Freydier, R. (2010) High-Precision Determination of the Isotopic Composition of Dissolved Iron in Iron Depleted Seawater by Double Spike Multicollector-ICPMS. Anal. Chem. 82, 7103-7111.

Le Quéré, C., Andres, R.J., Boden, T., Conway, T., Houghton, R.A., House, J.I., Marland, G., Peters, G.P., van der Werf, G.R., Ahlström, A., Andrew, R.M., Bopp, L., Canadell, J.G., Ciais, P., Doney, S.C., Enright, C., Friedlingstein, P., Huntingford, C., Jain, A.K., Jourdain, C., Kato, E., Keeling, R.F., Klein Goldewijk, K., Levis, S., Levy, P., Lomas, M., Poulter, B., Raupach, M.R., Schwinger, J., Sitch, S., Stocker, B.D., Viovy, N., Zaehle, S. and Zeng, N. (2013) The global carbon budget 1959–2011. Earth Syst. Sci. Data 5, 165-185.

Liu, X. and Millero, F.J. (2002) The solubility of iron in seawater. Mar. Chem. 77, 43-54.

Lomnitz, U. (2017) Biogeochemical cycling of iron and phosphorus under low oxygen conditions, Mathematisch-Naturwissenschaftliche Fakultät. Christian-Albrechts-Universität zu Kiel, Kiel.

Mackey, D.J., O'Sullivan, J.E.O. and Watson, R.J. (2002) Iron in the western Pacific: a riverine or hydrothermal source for iron in the Equatorial Undercurrent? Deep Sea Research Part I: Oceanographic Research Papers 49, 877-893.

Marsay, C.M., Sedwick, P.N., Dinniman, M.S., Barrett, P.M., Mack, S.L. and McGillicuddy, D.J. (2014) Estimating the benthic efflux of dissolved iron on the Ross Sea continental shelf. Geophysical Research Letters 41, 7576-7583.

Martin, J.H. (1990) Glacial-interglacial CO2 change: the iron hypothesis. Paleoceanography 5, 1-13.

Martin, J.H. and Fitzwater, S.E. (1988) Iron-deficiency limits phytoplankton growth in the northeast Pacific Subarctic. Nature 331, 341-343.

Martin, J.H., Knauer, G.A., Karl, D.M. and Broenkow, W.W. (1987) VERTEX: carbon cycling in the northeast Pacific. Deep Sea Research Part A. Oceanographic Research Papers 34, 267-285.

Mead, C., Herckes, P., Majestic, B.J. and Anbar, A.D. (2013) Source apportionment of aerosol iron in the marine environment using iron isotope analysis. Geophysical Research Letters 40, 5722-5727.

Measures, C.I. and Brown, E.T. (1996) Estimating dust input to the Atlantic Ocean using surface water Al concentrations, in: Guerzoni, S., Chester, R. (Eds.), The Impact of Desert Dust Across the Mediterranean. Kluwer Academic Publishers, Dortrecht, p. 389.

Millero, F.J., Sotolongo, S. and Izaguirre, M. (1987) The oxidation-kinetics of Fe(II) in seawater. Geochim. Cosmochim. Acta 51, 793-801.

Milne, A., Schlosser, C., Wake, B.D., Achterberg, E.P., Chance, R., Baker, A.R., Forryan, A. and Lohan, M.C. (2017) Particulate phases are key in controlling dissolved iron concentrations in the (sub)tropical North Atlantic. Geophysical Research Letters 44, 2377-2387.

Monterey, G.I. and Levitus, S. (1997) Seasonal variability of mixed layer depth for the world ocean. US Department of Commerce, National Oceanic and Atmospheric Administration, National Environmental Satellite, Data, and Information Service.

Moore, J.K., Doney, S.C., Glover, D.M. and Fung, I.Y. (2001) Iron cycling and nutrient-limitation patterns in surface waters of the World Ocean. Deep Sea Research Part II: Topical Studies in Oceanography 49, 463-507.

Moran, S.B. and Moore, R.M. (1992) Kinetics of the removal of dissolved aluminum by diatoms in seawater: A comparison with thorium. Geochim. Cosmochim. Acta 56, 3365-3374.

Morgan, J.L.L., Wasylenki, L.E., Nuester, J. and Anbar, A.D. (2010) Fe Isotope Fractionation during Equilibration of Fe-Organic Complexes. Environmental Science & Technology 44, 6095-6101.

Nishioka, J. and Obata, H. (2017) Dissolved iron distribution in the western and central subarctic Pacific: HNLC water formation and biogeochemical processes. Limnol. Oceanogr., n/a-n/a.

Noffke, A., Hensen, C., Sommer, S., Scholz, F., Bohlen, L., Mosch, T., Graco, M. and Wallmann, K. (2012) Benthic iron and phosphorus fluxes across the Peruvian oxygen minimum zone. Limnol. Oceanogr. 57, 851-867.

Patey, M.D., Achterberg, E.P., Rijkenberg, M.J. and Pearce, R. (2015) Aerosol time-series measurements over the tropical Northeast Atlantic Ocean: Dust sources, elemental composition and mineralogy. Mar. Chem. 174, 103-119.

Planquette, H., Statham, P.J., Fones, G.R., Charette, M.A., Moore, C.M., Salter, I., Nedelec, F.H., Taylor, S.L., French, M., Baker, A.R., Mahowald, N. and Jickells, T.D. (2007) Dissolved iron in the vicinity of the Crozet Islands, Southern Ocean. Deep-Sea Res. Part II-Top. Stud. Oceanogr. 54, 1999-2019.

Poitrasson, F., Vieira, L.C., Seyler, P., Pinheiro, G.M.D., Mulholland, D.S., Bonnet, M.P., Martinez, J.M., Lima, B.A., Boaventura, G.R., Chmeleff, J., Dantas, E.L., Guyot, J.L., Mancini, L., Pimentel, M.M., Santos, R.V., Sondag, F. and Vauchel, P. (2014) Iron isotope composition of the bulk waters and sediments from the Amazon River Basin. Chem. Geol. 377, 1-11.

Radic, A., Lacan, F. and Murray, J.W. (2011) Iron isotopes in the seawater of the equatorial Pacific Ocean: New constraints for the oceanic iron cycle. Earth. Planet. Sci. Lett. 306, 1-10.

Resing, J.A. and Measures, C.I. (1994) Fluorometric determination of Al in seawater by Flow-Injection-Analysis with in-line preconcentration. Anal. Chem. 66, 4105-4111.

Resing, J.A., Sedwick, P.N., German, C.R., Jenkins, W.J., Moffett, J.W., Sohst, B.M. and Tagliabue, A. (2015) Basin-scale transport of hydrothermal dissolved metals across the South Pacific Ocean. Nature 523, 200-203.

Rijkenberg, M.J.A., Middag, R., Laan, P., Gerringa, L.J.A., van Aken, H.M., Schoemann, V., de Jong, J.T.M. and de Baar, H.J.W. (2014) The distribution of dissolved iron in the west atlantic ocean. PloS one 9, e101323-e101323.

Rijkenberg, M.J.A., Steigenberger, S., Powell, C.F., van Haren, H., Patey, M.D., Baker, A.R. and Achterberg, E.P. (2012) Fluxes and distribution of dissolved iron in the eastern (sub-) tropical North Atlantic Ocean. Global Biogeochem. Cycles 26.

Rouxel, O., Shanks, W.C., Bach, W. and Edwards, K.J. (2008) Integrated Fe- and S-isotope study of seafloor hydrothermal vents at East Pacific rise 9-10 degrees N. Chem. Geol. 252, 214-227.

Schlosser, C., Klar, J.K., Wake, B.D., Snow, J.T., Honey, D.J., Woodward, E.M.S., Lohan, M.C., Achterberg, E.P. and Moore, C.M. (2014) Seasonal ITCZ migration dynamically controls the location of the (sub)tropical Atlantic biogeochemical divide. Proceedings of the National Academy of Sciences 111, 1438-1442.

Schmidtko, S., Stramma, L. and Visbeck, M. (2017) Decline in global oceanic oxygen content during the past five decades. Nature 542, 335-339.

892 Schott, F.A., McCreary, J.P. and Johnson, G.C. (2004) Shallow Overturning Circulations of the
893 Tropical-Subtropical Oceans, Earth's Climate. American Geophysical Union, pp. 261-304.

894 Severmann, S., Johnson, C.M., Beard, B.L. and McManus, J. (2006) The effect of early
895 diagenesis on the Fe isotope compositions of porewaters and authigenic minerals in continental
896 margin sediments. Geochim. Cosmochim. Acta 70, 2006-2022.

897 Severmann, S., McManus, J., Berelson, W.M. and Hammond, D.E. (2010) The continental shelf
898 benthic iron flux and its isotope composition. Geochim. Cosmochim. Acta 74, 3984-4004.

899 Siedlecki, S.A., Mahadevan, A. and Archer, D.E. (2012) Mechanism for export of sediment-
900 derived iron in an upwelling regime. Geophysical Research Letters 39.

901 Siedler, G., Kuhl, A. and Zenk, W. (1987) The Madeira mode water. J. Phys. Oceanogr. 17, 1561-
902 1570.

903 Stramma, L., Brandt, P., Schafstall, J., Schott, F., Fischer, J. and Koertzinger, A. (2008a) Oxygen
904 minimum zone in the North Atlantic south and east of the Cape Verde Islands. J. Geophys. Res.-
905 Oceans 113.

906 Stramma, L. and England, M. (1999) On the water masses and mean circulation of the South
907 Atlantic Ocean. Journal of Geophysical Research: Oceans 104, 20863-20883.

908 Stramma, L., Huttl, S. and Schafstall, J. (2005) Water masses and currents in the upper tropical
909 northeast Atlantic off northwest Africa. J. Geophys. Res.-Oceans 110.

910 Stramma, L., Johnson, G.C., Sprintall, J. and Mohrholz, V. (2008b) Expanding oxygen-minimum
911 zones in the tropical oceans. Science 320, 655-658.

912 Stramma, L. and Schott, F. (1999) The mean flow field of the tropical Atlantic Ocean. Deep-Sea
913 Res. Part II-Top. Stud. Oceanogr. 46, 279-303.

914 Tagliabue, A., Bowie, A.R., Boyd, P.W., Buck, K.N., Johnson, K.S. and Saito, M.A. (2017) The
915 integral role of iron in ocean biogeochemistry. Nature 543, 51-59.

916 Taylor, S.R. (1964) Abundance of chemical elements in the continental crust: a new table.
917 Geochim. Cosmochim. Acta 28, 1273-1285.

918 Twining, B.S., Rauschenberg, S., Morton, P.L. and Vogt, S. (2015) Metal contents of
919 phytoplankton and labile particulate material in the North Atlantic Ocean. Prog. Oceanogr. 137, Part
920 A, 261-283.

Ussher, S.J., Achterberg, E.P., Powell, C., Baker, A.R., Jickells, T.D., Torres, R. and Worsfold, P.J. (2013) Impact of atmospheric deposition on the contrasting iron biogeochemistry of the North and South Atlantic Ocean. Global Biogeochem. Cycles 27, 1096-1107.

Ussher, S.J., Achterberg, E.P., Sarthou, G., Laan, P., de Baar, H.J.W. and Worsfold, P.J. (2010) Distribution of size fractionated dissolved iron in the Canary Basin. Marine Environmental Research 70, 46-55.

Ussher, S.J., Achterberg, E.P. and Worsfold, P.J. (2004) Marine Biogeochemistry of Iron. Environmental Chemistry 1, 67-80.

Waeles, M., Baker, A.R., Jickells, T. and Hoogewerff, J. (2007) Global dust teleconnections: aerosol iron solubility and stable isotope composition. Environmental Chemistry 4, 233-237.

Woodward, E.M.S. and Rees, A.P. (2001) Nutrient distributions in an anticyclonic eddy in the northeast Atlantic Ocean, with reference to nanomolar ammonium concentrations. Deep-Sea Res. Part II-Top. Stud. Oceanogr. 48, 775-793.

Table 1

Sample ID	Depth (m)	σ_θ (kg m^{-3})	Oxygen (µmol kg^{-1})	Salinity	pot T (°C)	water mass	dFe (nmol L^{-1})	2 SD (nmol L^{-1})	δ^{56}Fe (‰)	2 SD (‰)	Phosphate (µmol L^{-1})	Nitrate (µmol L^{-1})
Station 4, Cast 11, 12.6120 N, -17.5728 E, 51 m bottom depth												
11_12	25	25.66	158.5	35.71	18.61	TSW	2.5	0.2	0.03	0.04	0.97	13.51
11_11	38	25.79	119.8	35.69	18.01	TSW	3.36	0.08	-0.20	0.04	1.08	15.76
11_10	40	25.83	111.6	35.68	17.84	TSW	3.49	0.16	-0.32	0.04	1.12	16.14
11_09	49	25.91	93.1	35.67	17.48	SACW	3.82	0.06	-0.25	0.04	1.13	6.68
Station 5, Cast 12, 12.5882 N, -17.5724 E, 164 m bottom depth												
12_23	26	25.72	138.4	35.69	18.34	TSW	3.01	0.10	-0.11	0.05	1.10	15.48
12_21	36	25.79	116.8	35.68	18.01	TSW	2.99	0.13	-0.23	0.05	1.21	17.26
12_19	51	25.88	96.9	35.67	17.63	SACW	3.5	0.2	-0.16	0.05	1.25	18.03
12_17	66	25.93	81.2	35.66	17.37	SACW	3.75	0.06	-0.25	0.04	1.25	18.08
12_15	80	25.96	78.5	35.66	17.23	SACW	3.68	0.09	-0.31	0.05	1.29	18.89
12_13	107	26.18	68.8	35.62	16.22	SACW	6.3	0.5	-0.33	0.05	1.43	21.51
Station 3, Cast 8, 12.6100 N, -17.7157 E, 1041 m bottom depth												
8_21	199	26.54	71.9	35.44	13.94	SACW	1.81	0.02	0.06	0.08	1.59	25.63
8_20	300	26.85	59.3	35.39	12.22	SACW	2.58	0.02	-0.15	0.08	1.73	28.62
8_19	400	27.03	44.6	35.27	10.76	SACW	2.86	0.08	-0.19	0.04	1.98	32.82
8_18	500	27.14	48.9	35.10	9.38	SACW/AAIW	3.77	0.19	-0.32	0.04	2.17	34.79
8_17	599	27.21	60.1	34.89	7.83	AAIW	2.14	0.09	-0.08	0.04	2.33	36.72
8_16	699	27.28	74.0	34.84	7.08	AAIW	2.66	0.05	-0.30	0.04	1.91	30.81
8_14	899	27.38	99.5	34.79	6.06	AAIW	2.69	0.06	-0.26	0.04	2.32	34.88
8_13	1002	27.50	130.8	34.84	5.38	AAIW	2.90	0.18	-0.27	0.04	2.16	31.77
									-0.21	0.08		
Station 2, Cast 6, 12.5942 N, -17.9199 E, 2656 m bottom depth												
6_21	198	26.63	70.5	35.41	13.39	SACW	1.85	0.10	-0.06	0.08	1.62	26.69
6_20	299	26.86	58.1	35.38	12.07	SACW	1.89	0.05	0.02	0.08	1.81	30.37
6_19	399	27.03	43.8	35.27	10.75	SACW	1.51	0.08	0.21	0.04	1.98	33.18
6_18	499	27.14	49.7	35.14	9.52	SACW/AAIW	1.40	0.04	0.41	0.04	2.19	35.37
6_17	599	27.22	58.5	34.93	7.93	AAIW	1.96	0.06	0.10	0.08	2.32	36.89
6_16	750	27.32	85.0	34.78	6.46	AAIW	1.82	0.05	0.12	0.08	2.37	36.55
									0.12	0.05		
6_15	900	27.40	111.1	34.76	5.64	AAIW	1.74	0.05	0.09	0.08	2.32	34.61
6_12	1699	27.77	216.9	34.96	3.82	NADW	1.66	0.03	0.12	0.08	1.60	22.76
6_10	2625	27.86	237.6	34.94	2.77	NADW	1.33	0.03	0.09	0.04	1.56	21.18

Table 2

Sample ID	Lat (°N)	Long (°E)	Stn	SMLD (m)	dAl_{meas} (nmol L^{-1})	SD	dFe_{meas} (nmol L^{-1})	SD	dFe_{dust} (nmol L^{-1})	SD	dust flux (µmol dFe m^{-2} d^{-1})	SD
F-44	12.590	-17.653	4 & 5	11	0.9	0.4	0.48	0.03	0.29	0.12	0.17	0.14
F-45	12.587	-17.714	3	19	2.1	0.4	0.45	0.02	0.70	0.13	0.71	0.50
F-46	12.586	-17.773	0	11	1.0	0.4			0.34	0.14	0.20	0.16
F-47	12.586	-17.831	0	11	2.4	0.4	0.76	0.02	0.78	0.14	0.46	0.32
F-48	12.585	-17.890	2	11	1.1	0.4	0.73	0.09	0.38	0.12	0.22	0.17
F-49	12.585	-17.949	0	11	2.1	0.4	0.83	0.03	0.70	0.12	0.41	0.29

Figure 1

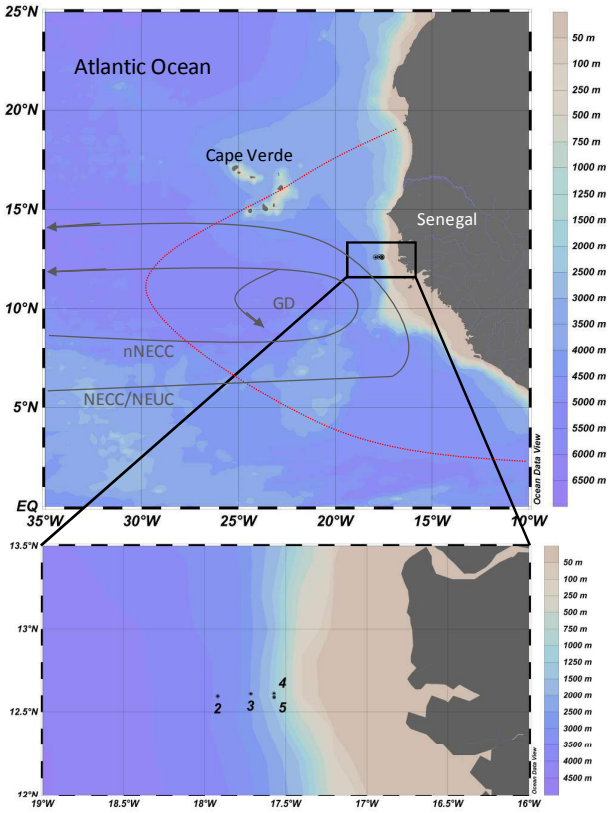
Atlantic Ocean
Cape Verde
Senegal
GD
nNECC
NECC/NEUC
25°N
20°N
15°N
10°N
5°N
EQ
35°W
30°W
25°W
20°W
15°W
10°W
50 m
100 m
250 m
500 m
750 m
1000 m
1250 m
1500 m
2000 m
2500 m
3000 m
3500 m
4000 m
4500 m
5000 m
5500 m
6000 m
6500 m
Ocean Data View
13.5°N
13°N
12.5°N
12°N
19°W
18.5°W
18°W
17.5°W
17°W
16.5°W
16°W
2
3
4
5

Figure 2

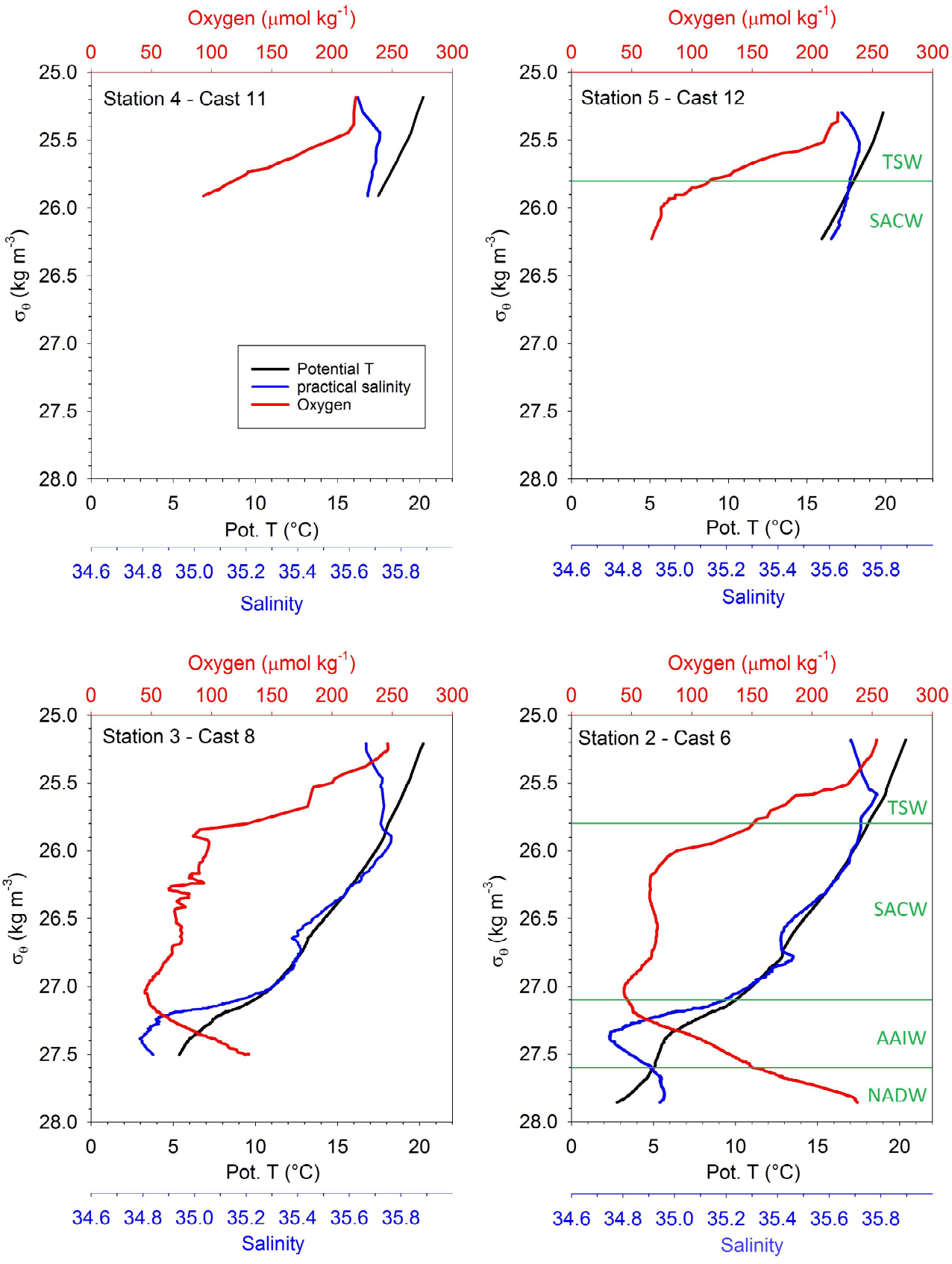
Oxygen (μmol kg-1)
0 50 100 150 200 250 300
Station 4 - Cast 11
Potential T
practical salinity
Oxygen
σθ (kg m-3)
25.0 25.5 26.0 26.5 27.0 27.5 28.0
0 5 10 15 20
Pot. T (°C)
34.6 34.8 35.0 35.2 35.4 35.6 35.8
Salinity
Station 5 - Cast 12
TSW
SACW
Station 3 - Cast 8
Station 2 - Cast 6
AAIW
NADW

Figure 3

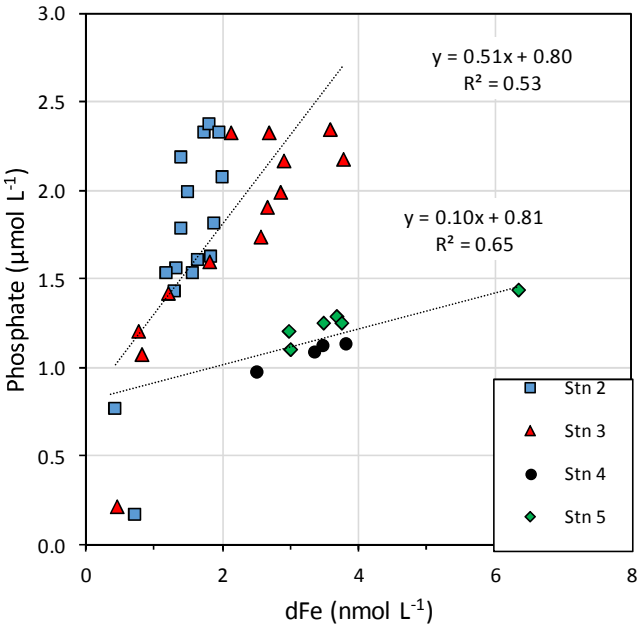
y = 0.51x + 0.80
R² = 0.53
y = 0.10x + 0.81
R² = 0.65
Stn 2
Stn 3
Stn 4
Stn 5
Phosphate (µmol L-1)
dFe (nmol L-1)
3.0
2.5
2.0
1.5
1.0
0.5
0.0
0
2
4
6
8

Figure 4

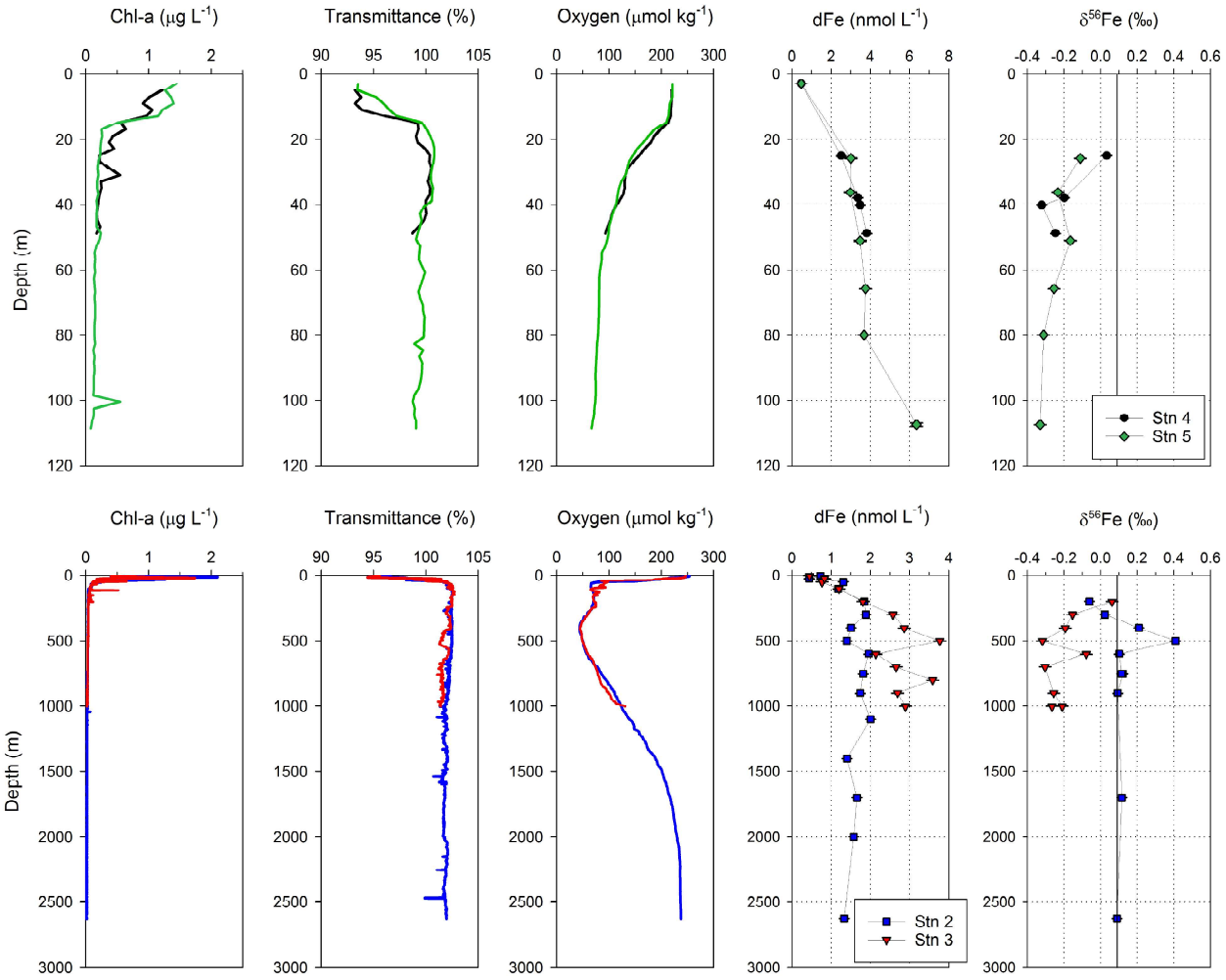
Chl-a (µg L-1)
Transmittance (%)
Oxygen (µmol kg-1)
dFe (nmol L-1)
δ56Fe (‰)
Depth (m)
Stn 4
Stn 5
Chl-a (µg L-1)
Transmittance (%)
Oxygen (µmol kg-1)
dFe (nmol L-1)
δ56Fe (‰)
Depth (m)
Stn 2
Stn 3

Figure 5

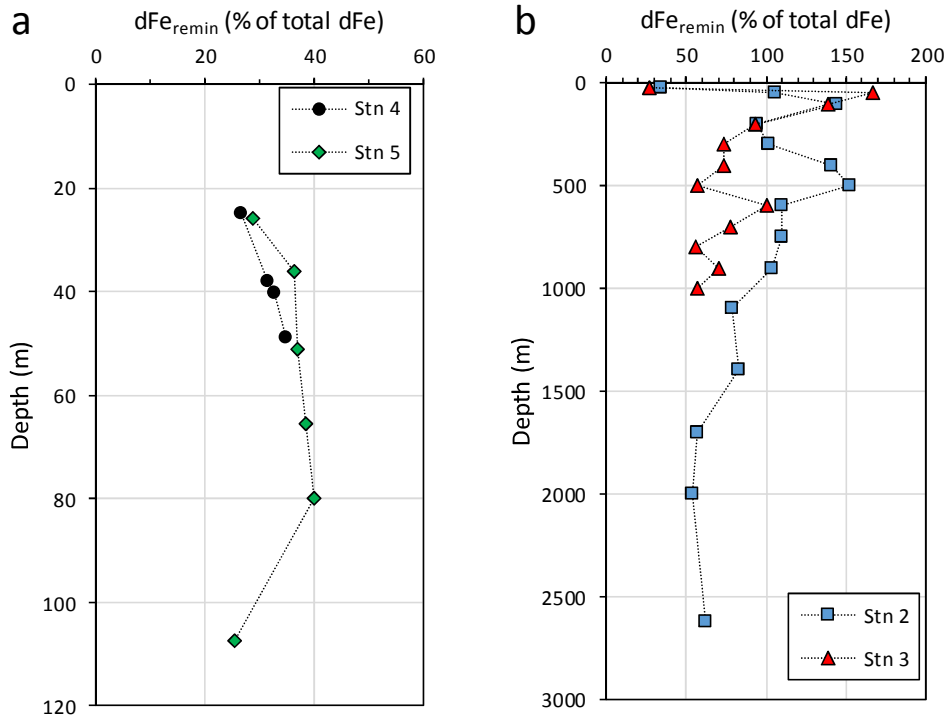
a
dFe$_{remin}$ (% of total dFe)
0
20
40
60
Depth (m)
0
20
40
60
80
100
120
Stn 4
Stn 5
b
dFe$_{remin}$ (% of total dFe)
0
50
100
150
200
Depth (m)
0
500
1000
1500
2000
2500
3000
Stn 2
Stn 3

Figure 6

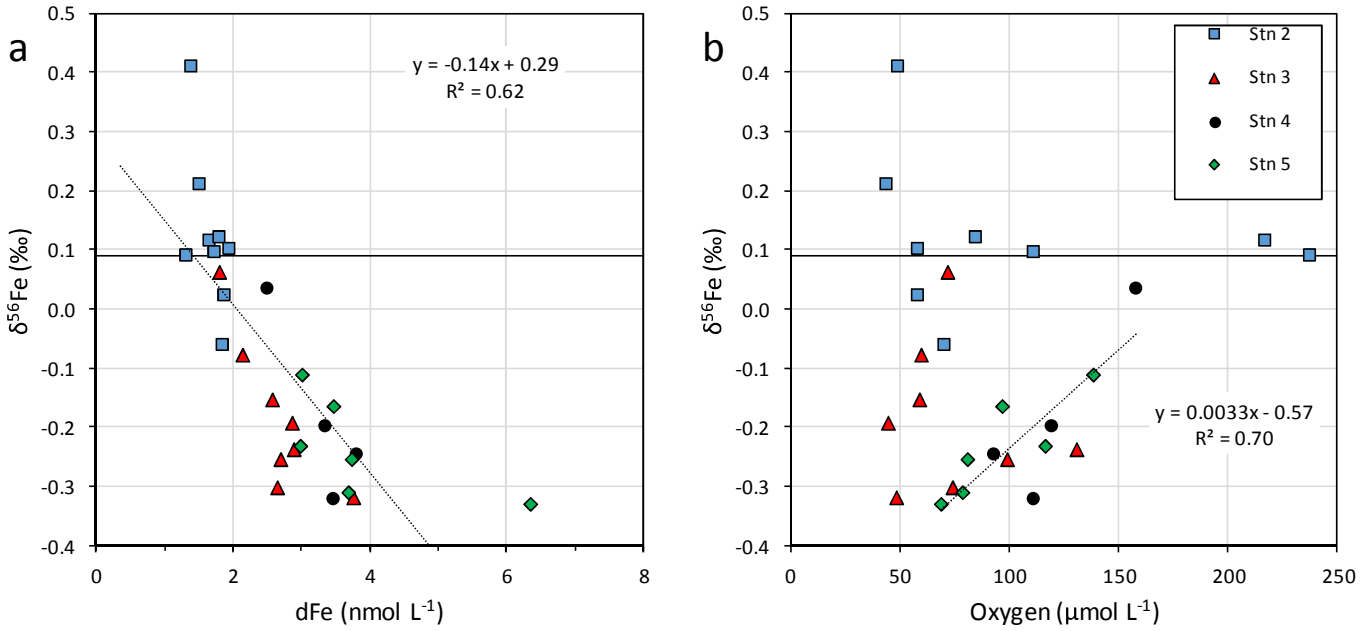
a
y = -0.14x + 0.29
R² = 0.62
δ56Fe (‰)
dFe (nmol L-1)
b
Stn 2
Stn 3
Stn 4
Stn 5
y = 0.0033x - 0.57
R² = 0.70
δ56Fe (‰)
Oxygen (µmol L-1)

Figure 7

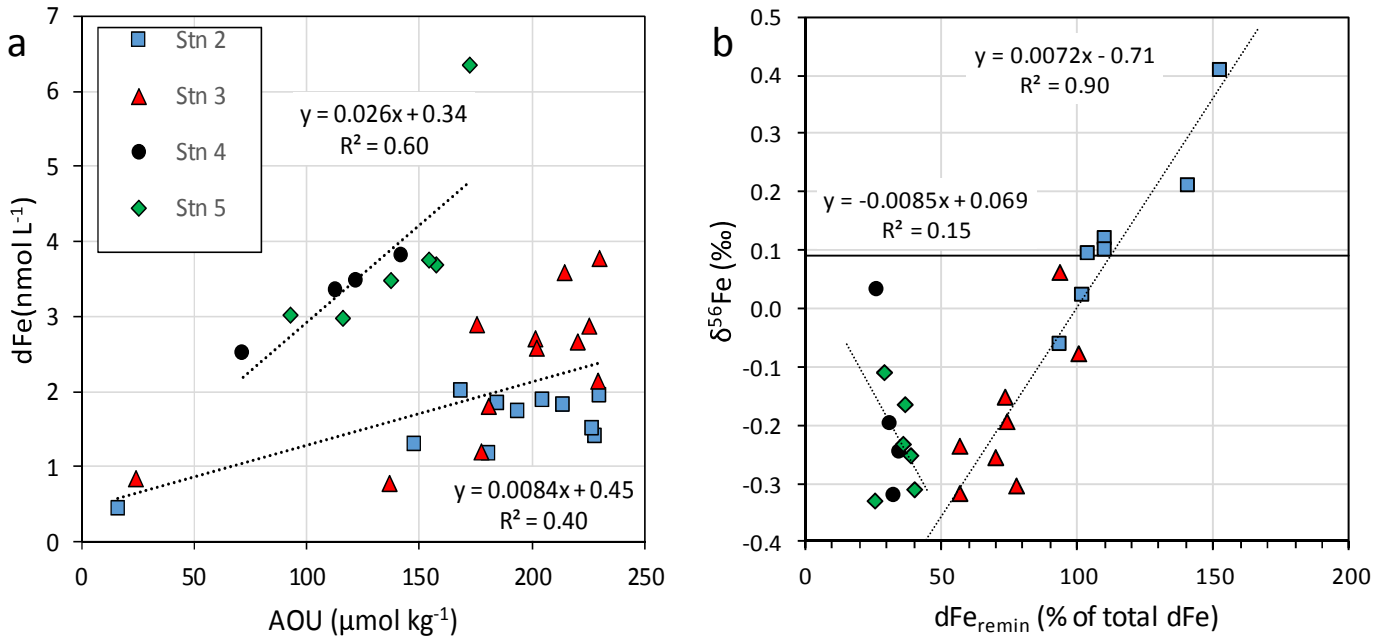
a
Stn 2
Stn 3
Stn 4
Stn 5
y = 0.026x + 0.34
R² = 0.60
y = 0.0084x + 0.45
R² = 0.40
dFe(nmol L-1)
AOU (µmol kg-1)
b
y = 0.0072x - 0.71
R² = 0.90
y = -0.0085x + 0.069
R² = 0.15
δ56Fe (‰)
dFeremin (% of total dFe)

Figure 8

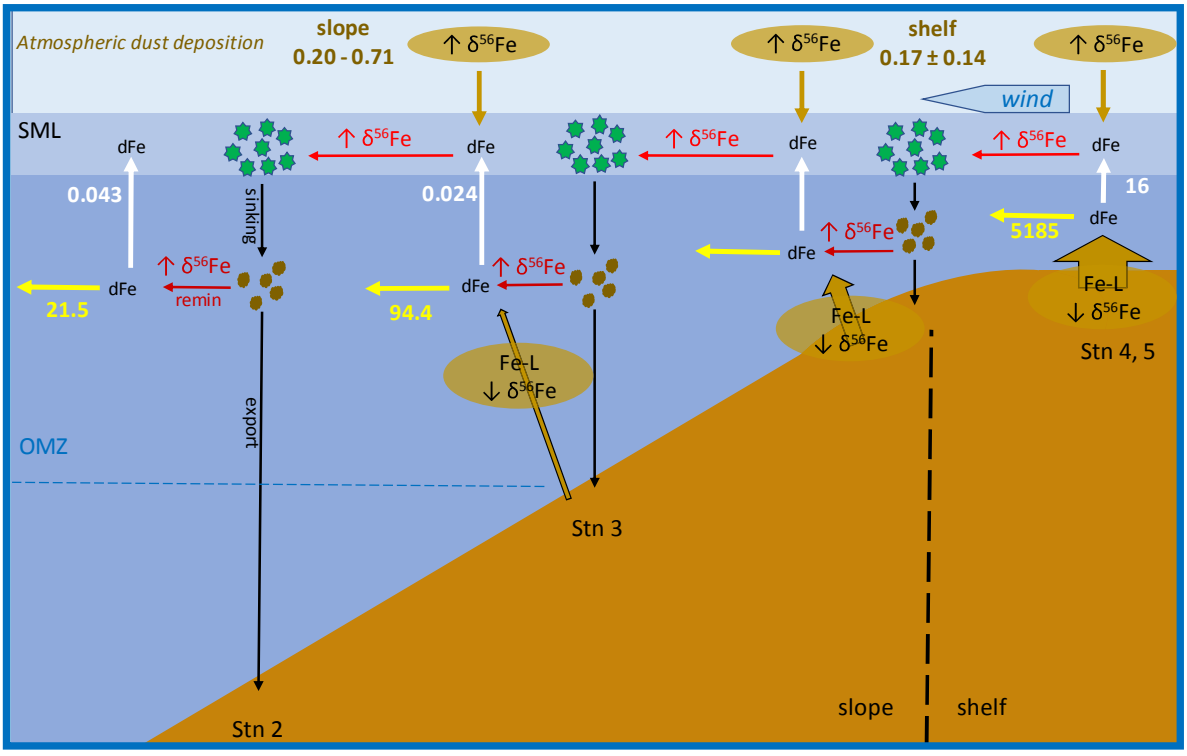
Atmospheric dust deposition
slope
0.20 - 0.71
↑ δ56Fe
↑ δ56Fe
shelf
0.17 ± 0.14
↑ δ56Fe
wind
SML
dFe
↑ δ56Fe
dFe
↑ δ56Fe
dFe
↑ δ56Fe
dFe
0.043
sinking
0.024
16
dFe
5185
↑ δ56Fe
dFe
dFe
↑ δ56Fe
remin
21.5
dFe
↑ δ56Fe
94.4
Fe-L
↓ δ56Fe
Fe-L
↓ δ56Fe
Fe-L
↓ δ56Fe
Stn 4, 5
OMZ
export
Stn 3
Stn 2
slope
shelf